Exosomal circZFR promotes colorectal cancer progression via interacting with BCLAF1 and regulating the miR-3127-5p/RTKN2 axis

Jiaxin Chen
Sir Run Run Shaw Hospital
Jianbin Xu
Sir Run Run Shaw Hospital
Huijuan Wang
Sir Run Run Shaw Hospital
Engeng Chen
Sir Run Run Shaw Hospital
Qing Meng
Sir Run Run Shaw Hospital
Jiawei Wang
Sir Run Run Shaw Hospital
Wei Zhou
Sir Run Run Shaw Hospital
Ge Shan
Sir Run Run Shaw Hospital
Zhenyu Ju
Jinan University
Zhangfa Song (songzhangfa@zju.edu.cn)
Sir Run Run Shaw Hospital

Research Article

Keywords: CRC, circZFR, exosome, ESRP1, BCLAF1, miR-3127-5p, RTKN2, nanoparticle (NP)

Posted Date: June 15th, 2022

DOI: https://doi.org/10.21203/rs.3.rs-1740013/v1

Abstract

Background

Circular RNAs (circRNAs) have gained attention as novel biomarkers for cancer diagnosis and prognosis. Aberrant expression of circRNAs is widely involved in cancer development, whereas the function and mechanism of novel circRNAs in colorectal cancer (CRC) remain unclear.

Methods

CircZFR was identified both in CRC tissues from the GEO database and in serum exosomes by competing endogenous RNA (ceRNA) microarray. The expression of circZFR was evaluated in CRC tissues and serum by qRT-PCR and in tissue microarray (TMA) by FISH. The functional roles were confirmed using a series of *in vitro* assays and tumor xenografts and pulmonary/hepatic metastasis mouse models. The mechanisms of circZFR were assessed through circRNA pulldown, RNA immunoprecipitation (RIP), dual-luciferase reporter assays and rescue experiments. Lastly, TCP1-CD-QDs nanocarrier was used to carry circZFR siRNA (si-circZFR) to exam the therapeutic potential of circZFR in patient-derived xenograft (PDX) models.

Results

CircZFR was upregulated in cancer tissues and serum exosomes of CRC patients and its level was positively associated to advanced TNM stages and poor prognosis. Serum circZFR was indicative of CRC incidence, advanced-stages and metastasis. Functional experiments demonstrated that circZFR promoted CRC proliferation and metastasis but inhibited apoptosis *in vitro* and *in vivo*, exosomes with upregulation of circZFR facilitated growth and migration of cocultured CRC cells. Mechanistically, the generation of circZFR could be improved by epithelial splicing regulatory protein 1 (ESRP1) in CRC cells. CircZFR bound to BCL2-associated transcription factor 1 (BCLAF1) and inhibited its ubiquitinated degradation. Moreover, circZFR sponged miR-3127-5p to increase the expression of rhotekin 2 (RTKN2). Our TCP1-CD-QDs nanocarrier was able to carry si-circZFR and delivered them to the vasculature of CRC tissues and cells, resulting in suppressive tumor growth without obvious adverse effects in PDX models.

Conclusions

Our findings indicate that ESRP1-mediated circZFR exerts oncogenic effects on CRC development and spread through suppressing BCLAF1 degradation and regulating the miR-3127-5P/RTKN2 axis. CircZFR is a promising serum biopsy marker for CRC diagnosis and an attractive target for further therapy.

Background

Colorectal cancer (CRC) remains the third most commonly diagnosed cancer and the second leading cause of cancer-related deaths throughout the world[1]. In recent years, the overall incidence of CRC has increased in individuals younger than 50 years old but the cause is largely unknown[2]. Although the control of risk factors and early detection by screening have contributed to the declining trend in the incidence and mortality, the proportion of CRC cases diagnosed at an advanced stage is still high[3]. Metastasis and recurrence are still the most primary reasons of CRC-associated death[4]. It is hoped that advances in unravelling the functional mechanisms underlying CRC development and spread will provide possible cure.

Over the past decade, circRNAs have emerged as a large class of transcripts characterized by a covalently closed-loop structure, many of which play critical roles in cancer initiation and progression because of their versatile roles in promotion of cancer proliferation and metastasis[5], remodeling of tumor microenvironment (TME), and regulation of immune response[6]. The inaugural mechanism of circRNA functions is described as microRNA (miR) sponges, then, additional mechanisms of action have been detected including protein sponge or decoys, protein recruitment, protein function enhancer or protein scaffolds[7, 8]. Moreover, a few circRNAs have been reported to possess coding potential and can function through circRNA-specific peptides[9]. As reported, circRNA could exert multiple functions in cancer progression through the combined action of different mechanisms[10–15]. For instance, circCD44 promotes triple-negative breast cancer (TNBC) progression via modulating the miR-502-5p/KRAS and insulin-like growth factor 2 mRNA binding protein 2(IGF2BP2)/Myc axes[13]. In addition, hsa_circ_0003258 drives prostate cancer development by sponging miR-653-5p and binding to IGF2BP3[10].

Intriguingly, circRNAs have also been shown to be enriched in serum exosomes and to have the potential as relatively non-invasive circulating biomarkers for cancer biopsies[16]. Exosomes are small membrane vesicles (40–160 nm) that released from most cell types especially tumor cells[17]. Although increasing studies have illustrated the pathological functions of exosomal circRNAs (exo-circRNAs) in various types of cancers, challenges still exist in multiple aspects in their clinical translation[18, 19]. Therefore, exo-circRNAs is a relatively young field of research that need further investigation.

The critical roles of circRNAs in oncology identify them as promising targets for novel anticancer therapy[20]. In previous study, we bound an adamantane (ADA)-modified TCP1 peptide-targeting ligand to the β-cyclodextrin (CD)-attached quantum dot (QD)-based nanoparticles (NPs) through host-guest interactions, this novel CRC-targeting NPs could carry both chemotherapeutic drugs and nucleotide drugs for synergistic therapy[21]. In this study, we evaluated the capacity of circZFR as a diagnostic and prognostic biomarker for CRC, explored how circZFR was generated and proved its oncogenic functions and mechanisms. Finally, we used TCP1-CD-QDs to assist the delivery of si-circZFR and assessed the potential of circZFR as a therapeutic target.

Methods

Clinical specimens

All 83 pairs of CRC tissues and corresponding adjacent normal tissues were obtained from CRC patients during operation between March 2019 and March 2021 at the Sir Run Run Shaw Hospital, Hangzhou, China. All 83 peripheral serum samples were collected from patients with CRC before operation between November 2018 and December 2020 at the Sir Run Run Shaw Hospital, Hangzhou, China. The inclusion criteria of patients were as follows: primary CRC with clear pathological diagnosis, no preoperative treatment including systemic chemotherapy and local radiotherapy, and complete clinicopathological records. Nevertheless, many patients that provided serum samples were diagnosed at advanced stages and had no indication for surgery. Therefore, clinicopathological features including tumor differentiation, lymphovascular or nerve invasion, and tumor size were unable to collected. Meanwhile, another 83 serum samples were also collected from sex- and age- matched healthy donors who underwent physical examination in the Sir Run Run Shaw Hospital during the same time period. The exclusion criteria of healthy population were as follows: diabetes, chronic systemic disease and obesity. For the construction of tissue microarray (TMA), 180 pairs of CRC and adjacent normal tissues were collected from patients with complete follow-up data during operation between October 2011 and August 2012 at the Sir Run Run Shaw Hospital.

The CRC stage was defined following the rules of the 8th edition of the American Joint Committee on Cancer (AJCC) tumor-node-metastasis (TNM) staging system. Among the 83 cancer serum samples, 3 stage □ and 3 stage □ samples were used for ceRNA microarray. All tissue and serum samples were collected with informed consent of patients and healthy donors and immediately stored at -80°C until use. This study was approved and monitored by the Ethics Committee of the Sir Run Run Shaw Hospital, Zhejiang University.

Cell culture and treatment

A panel of CRC cell lines, including HCE8693, SW480, SW620, DLD-1, RKO, Colo320 and HCT116, and human embryonic kidney cells (HEK-293T, referred to as 293T hereafter) were cultured in Dulbecco's modified essential medium (DMEM) or RPML-1640 medium (Gibco BRL, Rockville, MD) with 100 μg/mL streptomycin, 100 U/mL penicillin and 10% fetal bovine serum (FBS; Gibco, NY, USA) and incubated at 37°C in a 5% humidified CO_2 atmosphere. Cells were treated with cycloheximide (CHX; Sigma, MO, USA) at 50 μg/mL for the indicated time period, MG132 or Chloroquine (Selleck Chemicals, Shanghai, China) at 20 μM or 10μM, respectively, for 12 h, PR619 (Selleck Chemicals, Shanghai, China) at 20 μM for 48–72 h.

Protocol for the isolation of cancer-associated fibroblasts (CAFs) and normal fibroblasts (NFs) derived from fresh CRC tissues and paired normal tissues was fully described in our published article[22].

Competing endogenous RNA (ceRNA) microarray

The ceRNA microarray were conducted according to the protocol of Agilent technologies at LC Sciences Corporation (Hangzhou, China). Total RNA was isolated and purified by using RNA Isolation Kit (Norgen

Biotek, Thorold, Canada) and RNase Mini Kit (Qiagen, Duesseldorf, Germany). The RIN number was then checked to inspect RNA integration by an Agilent Bioanalyzer 2100 (Santa Clara, CA, USA). Next, exosomal RNA samples of m-CRCs and n-CRCs were used for the LC Human ceRNA Array V1.0 to generate biotinylated cRNA targets which hybridized with the sliders. After hybridization, sliders were scanned on the Agilent Microarray Scanner (Santa Clara, CA, USA). Finally, data were extracted with Feature Extraction software (Santa Clara, CA, USA) and normalized by Quantile algorithm.

RNA extraction and quantitative reverse transcription polymerase chain reaction (qRT-PCR)

Total RNA was extracted from tissues, serum or cells using the TRIzol reagent (Invitrogen, MA, USA), and RNA concentration was measured by Nanodrop 2000. RNA was treated with 3 U/μg RNase R (Epicenter Technologies, Madison, WI, USA) for 15 min at 37°C, or 5 μg/mL actinomycin D (AAT Bioquest, CA, USA) and collected at the indicated time points. Then, RT-qPCR were performed using an Evo M-MLV RT Premix kit (Accurate Biotechnology (Hunan) Co., Ltd) and SYBR FAST Universal qPCR kit (KAPA, Wilmington, USA) as described in our published article[22].

Exosome isolation and characterization

Exosomes were isolated from serum and culture medium of CRC cells following the standard centrifugation steps. Firstly, centrifugation at 300 g for 10 min, followed by 2000 g for 10 min, and 10,000 g for 30 min. The supernatant was then filtered to an ultracentrifuge and centrifuged at 100,000 g for 70 min at 4°C twice to pellet the exosomes. Finally, exosomes were resuspended in PBS (usually 50 μL to 100 μL).

The shape and size of exosomes were observed by transmission electron microscopy (TEM) and size distribution of exosomes was detected by dynamic light scattering (DLS). The characterization of the isolated exosomes was confirmed by the expression of exosomal protein marker tumor susceptibility 101 (TSG101), CD63 and CD81.

Fluorescence in situ hybridization (FISH)

Digoxigenin (DIG)-labeled circZFR probes and Cy3-labled miR-3127-5p probes were designed and synthesized by RiboBio (Guangzhou, China). The FISH Kit (RiboBio, Guangzhou, China) was utilized for testing the expression and localization of circZFR and miR-3127-5p in CRC cells and the expression and localization of circZFR in TMA following the manufacturer's guidelines. Images were captured under a fluorescence microscopy (Nikon, Tokyo, Japan) and the FISH signals were scored using Image-Pro Plus 6.0 (Media Cybernetics, Inc., Rockvile, MD, USA) software to obtain the average optical density of each photo.

SiRNA transfection and Lentivirus stable transduction

The human CRC cell lines HCT116 and Colo320, or 293T were seeded 40% confluent in 6-well or 24-well plates overnight. Small interfering RNAs (siRNAs) of circZFR (RiboBio, Guangzhou, China), miRNA

mimics and inhibitors (GenePharma, Shanghai, China) were transfected by Lipofectamine RNAiMax (Invitrogen, CA, USA) following the manufacturer's protocol. To construct small hairpin RNA (shRNA) or overexpression lentivirus plasmid, the sequence of si-circZFR or circZFR was cloned into the pHBLV-U6-MCS-CMV-ZsGreen-PGK-PURO vector or pHBLV-CMV-circ-EF1-ZsGreen-T2A-Puro vector (Hanbio Co. Ltd., Shanghai, China). The generation of lentivirus was achieved by co-transfection of the expression plasmid with the packaging plasmids psPAX2 and pMD2G using Lipofectamine 3000 (Invitrogen, CA, USA) according to the manufacturers' instructions. After transfection, positive cells were propagated in 2 μg/mL puromycin (Gibco, Grand Island, NY, USA) for one week and harvested for subsequent experiments.

5-Ethynyl-2'-deoxyuridine (EdU) and Cell counting kit-8 (CCK-8) assays

The proliferation rate of CRC cells was detected by the Cell-Light EdU DNA Cell Proliferation Kit (RiboBio, Guangzhou, China) and the CCK-8 solution (Dojindo Lab. Kumamoto, Japan). For the EdU assay, cells were seeded 30%-50% confluent in 24-well plates and cultured for 24 h. EdU solution (50 μM) was added to each well of plate and incubated for 2 h. The cells were then fixed with 4% formaldehyde for 20 min and permeabilized with 0.5% Triton 100 for 10 min. In the following step, Apollo Dye solution to stain the EdU for 30 min and Hoechst 33342 to stain the nuclei. Images were obtained with a Nikon microscope (Tokyo, Japan) and the proportion of EdU-positive cells was counted by Image J.

For the CCK-8 assay, seven thousand cells were seeded in 96-well plates and 10 μL of CCK-8 solution was added to each well at the appointed time. After a 2-h incubation at 37°C in a 5% humidified CO_2 atmosphere, the absorbance at 450 nm was measured with an automatic microplate reader (BioTek, Winooski, VT, USA). The EdU and CCK-8 experiments were performed in triplicate.

Soft agar colony formation assay

Primarily, semisolid agar medium (0.6% agarose/Phosphate buffer saline, PBS) was added onto the bottom layer of 6-well plates. Then, CRC cells were trypsinized and made into 25000 cells/mL suspension in culture medium. The mixture of CRC cells and semisolid agar medium (0.5% agarose/PBS) was added onto the bottom layer. After the gel was solidified, we added 1 mL culture medium on each well and changed the medium every 4 days. After at least 14 days of incubation, representative images of the cell colonies were obtained under microscope. The experiments were replicated at least three times.

Transwell, wound-healing and Cytoskeleton assays

Transwell migration and invasion assays, and wound-healing assay were carried out as previously reported[22].

To visualize the actin cytoskeleton, chamber slides were primarily added in 12-well plates and then CRC cells were seeded in plates for 24 h. The PBS-rinsed cells were fixed with 4% formaldehyde for 20 min, permeabilized with 0.5% Triton 100 for 10 min and blocked with bovine serum albumin (BSA; Fude Bio,

Hangzhou, China) for 1 h at room temperature. Alexa Fluor 594 Phalloidin (Thermo, Waltham, MA, USA) was used to mark Filament-actin (F-actin) to observe the cytoskeleton, and nuclei were stained with Hoechst 33342. Fluorescent imaging of cells was detected under an Olympus immunofluorescence microscope. All assays were independently performed in triplicate.

Apoptosis analysis

For detection of cell apoptosis, an Annexin V-FITC/propidium iodide (PI) Kit (BD Biosciences, SanDiego, USA) was used. CRC cells were isolated and washed with cold PBS for three times, then stained with Annexin V-FITC/PI at room temperature in the dark for at least 15 min. The apoptotic rate was analyzed using a flow cytometer (BD FACSCANTO Ⅱ, San Jose, USA) and FlowJo software. The experiments were repeated at least three times.

Western blotting and antibodies

Proteins in cells were extracted with RIPA lysis buffer (Fude Bio, Hangzhou, China). Western blotting experiments were performed according to details previously reported[22]. The primary antibodies used in this study are as follows: anti-E-cadherin (3195, Cell Signaling Technology, CST), anti-N-cadherin (sc-8424, Santa Cruz), anti-MMP9 (13667, CST), anti-Bcl-2 (4223, CST), anti-Bax (5023, CST), anti-cleaved caspase-9 (9509, CST), anti-cleaved caspase-3 (9661, CST), anti-β-actin (3700, CST), anti-TSG101 (ab133586, Abcam), anti-CD63 (ab134045, Abcam), anti-CD81 (ab109201, Abcam), anti-ESRP1 (21045-1-AP, proteintech), anti-BCLAF1 (ab181240, Abcam), anti-TF (17435-1-AP, proteintech), anti-DDX18 (ab128197, Abcam), anti-CAPN1 (2556, CST), anti-FLAG (14793, CST), anti-RTKN2 (Thermo, PA5-58392), anti-AGO-2 (MA5-23515, Thermo), anti-Ki67 (27309-1-AP, proteintech).

Biotin-labeled RNA pulldown and mass spectrometry (MS)

The 5’ biotin-labeled oligonucleotide probe targeting the junction site of circZFR was synthesized as follows: 5’- ACGACGUAAGGGCCAGCUUGGAAAAUCAG-3’. The biotin-labeled RNA probe was incubated with cell extracts from HCT116 cells stably transfected with N.C or circZFR overexpression vector. Then, the biotinylated circZFR-protein mixture was captured with Streptavidin Magnetic Beads and washed following the manufacturer’s protocol. The retrieved proteins were collected for Western blotting detection or silver staining (Beyotime, Shanghai, China) and mass spectrometry (MS) analysis.

RNA-protein immunoprecipitation (RIP) and IP

The RIP experiments were performed by using a Magna RNA-binding Protein Immunoprecipitation Kit (Millipore, Bedford, MA, USA) according to the manufacturer’s protocol. In brief, HCT116 extracts were incubated with protein A/G beads conjugated to an antibody against ESRP1 or BCLAF1 or AGO-2 and controlled by normal rabbit IgG (A01008, GenScript).

N.C/circZFR overexpressing HCT116 cells were transfected with FLAG-tagged BCLAF1 overexpression plasmid transiently by Lipofectamine 3000 (Invitrogen, CA, USA). After treatment of MG132 for 12 h, cells

were harvested and lysed, then incubated with anti-FLAG M2 Magnetic beads (Sigma, MO, USA). After rotating incubation overnight at 4°C, the bead-bound proteins were released and detected by Western blotting with an anti-ubiquitin antibody (3936, CST) according to the manufacturer's protocol.

Dual luciferase reporter assay

The binding between circZFR and miRs was detected by the Dual luciferase reporter Kit (Beyotime, Jiangsu, China). The wild type (WT) or mutant type (MUT) circZFR sequence was cloned into the PSI-Check2 vector (Hanbio Co. Ltd., Shanghai, China), which contains the firefly luciferase gene and Renilla luciferase gene. For the RTKN2 and miR-3127-5p experiments, WT or MUT RTKN2 3'UTR sequence was cloned to the PSI-Check2 vector. 293T or CRC cells were seeded 50% confluent in 24-well plates overnight and then cotransfected with circZFR-WT/MUT luciferase vector or RTKN2-WT/NUT luciferase vector and PSI-Check/miR mimics. After 24 h, the luciferase activity was measured according to the manufacture's protocol.

Animal studies

Firstly, luciferase-expressing HCT116 cells were stably transfected with N.C or sh-circZFR vectors to construct the N.C or sh-circZFR group. For the subcutaneous xenograft tumor model, 12 BALB/c nude mice (male, 4 weeks old) were randomly divided into 2 groups, and each was implanted subcutaneously in the flank site with 4×10^6 cells suspended in sterile PBS. Three weeks later, tumors were imaged using a Spectrum *in vivo* imaging system (IVIS) (PerkinElmer, USA). For the pulmonary metastasis model, 12 mice (male, 5 weeks old) were randomly divided into 2 groups, and each was injected into the tail vein with 2×10^6 cells suspended in sterile PBS. Tumors were imaged after four weeks. For the hepatic metastasis model, 12 mice (male, 6 weeks old) were randomly divided into 2 groups, 4×10^6 cells suspended in PBS were injected into the inferior of spleen. Tumors were imaged after five weeks. The *in vivo* imaging of mice was performed according to the previously described protocols[22]. After imaging, the mice were sacrificed and the tumors and organs including lung and liver were harvested and used for H&E and IHC staining according to the manufacturer's protocol. All the animal studies were approved by the Zhejiang University Animal Care and Use Committee and performed following the national guidelines and regulations.

To construct the PDX models, fresh CRC tissues were cut into 2 mm^3 pieces and washed twice with PBS and suspended in RPML 1640 medium containing penicillin and streptomycin. Then, the tumor specimens were placed in the flank of 15 nude mice. When the tumor volume reached 100 mm^3 (volume = 0.5 × $width^2$ × length), mice were randomly divided into 3 groups and intravenously injected with PBS, si-circZFR conjugated with cholesterol (Chol) or TCP1-CD-QDs loaded with si-circZFR every three days. The dosage of siRNA in the Chol-conjugated si-circZFR group and nanocarrier group were based on the loading capacity of TCP1-CD-QDs (2 mg/kg). After three weeks, the mice were sacrificed and tumors were harvested for further H&E and IHC staining. All patients provided consent to allow their tissues to be

stored and used for research. This study was approved and monitored by the Ethics Committee of the Sir Run Run Shaw Hospital, Zhejiang University.

Statistical analysis

Data are presented as the means ± standard deviations (SDs). Paired or unpaired two-tailed Student's t-tests and one-way ANOVA followed by Bonferroni tests were applied for the group comparison. Chi-square calculations or one-way ANOVA was used to assess the relationship between circZFR expression and clinicopathological characteristics of CRC patients from TMA. The receiver operating characteristic (ROC) curves were applied to assess the diagnostic capacity of circZFR in tissues and serum from CRC patients with different clinical characteristics. The Kaplan-Meier analysis was used to evaluate the effect of circZFR on the overall survival (OS) of CRC patients from TAM. Univariate Cox regression analysis was utilized to estimate hazard ratios (HRs) and corresponding 95% confidence intervals (CIs). The correlations between circZFR and ESRP1 or RTKN2 in CRC tissues was determined by Pearson's correlation analysis. Statistical analysis was performed by SPSS software and GraphPad Prism 8 software, and significance was set at $*p < 0.05$, $**p < 0.01$ and $***p < 0.001$.

Results

CircZFR is highly expressed in both CRC tissues and serum and represent a promising biomarker

To identify CRC-related functional circRNAs, we firstly performed bioinformatic analysis of a circRNA microarray consisting of ten pairs of CRC tissues and adjacent normal tissues from the GEO database (GSE126094). As a result, circZFR (has_circ_0072088) was the most highly upregulated circRNA in CRC tissues compared with normal tissues according to fold-change (FC) filtering (Fig. S1A). We then retrieved the TCGA database and found that the expression of zinc finger RNA binding protein (ZFR) mRNA (linZFR) was not significantly different between cancer and paired normal tissues (Fig. S1B). Given that exo-circRNAs have pivotal roles in cancer progression and metastasis, we then used ceRNA microarray to profile differentially expressed circRNAs in peripheral serum exosomes isolating from three metastatic CRC patients (m-CRCs) and three non-metastatic CRC patients (n-CRCs). The heatmap of significantly upregulated exo-circRNAs in m-CRCs compared to n-CRCs were shown in Fig. S1C according to FC > 2 and p value < 0.05. We found that circZFR was also enhanced in exosomes from m-CRCs, suggesting that circZFR might be associated with CRC metastasis. Therefore, circZFR with increased expression in CRC tissues and can be encapsulated in exosomes was chosen for further validation (Fig. 1A).

We measured circZFR levels in CRC tissues and paired benign tissues from 83 CRC patients and found that circZFR exhibited higher levels in 72 tumor tissues relative to adjacent non-malignant tissues (Fig. 1B). Interestingly, the expression of circZFR in cancer tissues was positively associated with tumor, node, metastasis (TNM) stage and distant metastasis (Fig. 1C, S1F-G). The ROC curve analysis demonstrated that tissue circZFR was indicative of distant metastasis but had relatively low diagnostic power as stage biomarker according to area under the curve (AUC) (Fig. S1F-G). The clinicopathological features of these

patients are shown in Fig. S1D. Tumor tissues consist of tumor cells and the surrounding stroma, which is predominantly constituted by CAFs[23]. To clarify the source of circZFR, we isolated primary CAFs and paired NFs from tissue samples of 10 CRC patients and found that circZFR levels has no significant difference between CAFs and NFs (Fig. S1E). Furthermore, the expression and location of circZFR were determined by FISH analysis in the TMA containing 180 pairs of CRC tissues and adjacent normal tissues. As the representative staining image of tissues from stage Ⅱ and stage Ⅲ patients shown in Fig. 1D, circZFR was markedly expressed at higher levels in CRC tissues than in nontumorous tissues with predominant distribution in epithelial cells but not stromal cells. In addition, CRC patients with higher circZFR levels exhibited shorter overall survival (OS) time (Fig. 1E). We then stratified the 180 patients from TMA into low and high groups based on circZFR levels in cancer tissues and found that high levels of circZFR were associated with tumor location, clinical stage and higher risk of developing lymph node and distant metastases (Table 1).

Considering the detection of upregulated circZFR in serum exosomes from m-CRCs compared to n-CRCs, we then tested circZFR levels in 83 paired serum samples from the general population and CRC patients. Consistent with the results in tissues, the abundance of circZFR in CRC serum was significantly enhanced compared to serum from healthy controls (Fig. 1F). Furthermore, the ROC curve revealed that serum circZFR is able to distinguish CRC patients from general population with AUC of 0.855 (Fig. 1G). As determined by qRT-PCR and ROC analysis, higher circZFR expression in serum were strongly indicative of advanced stages and distant metastasis (Fig. S1H-I). The clinicopathological characteristics of the 83 CRC patients who provided serum samples are shown in Fig. S1J. According to circBase, circZFR was consisted of exon 13-17 of ZFR gene and sequences in the back-splicing junction was evidenced by Sanger sequencing (Fig. 1H). To further confirm the traits of circZFR, we designed specific divergent primers for circZFR and convergent primers for linZFR and determined their expression, the results revealed that circZFR is a transcript from alternative splicing but not generated from genomic DNA (gDNA) (Fig. 1I). Then we performed a series of experiments to confirm the stability of circZFR and found that circZFR was relatively resistant to RNase R and Actinomycin D treatments compared to linZFR (Fig. 1J-K). Notably, FISH showed that circZFR was localized in both nuclear and cytoplasm of HCT116 and Colo320 cells with predominant expression in the cytoplasm (Fig. 1L, S1K).

Together, circZFR is upregulated in CRC tissues and can be delivered by exosomes into circulation. Tissue and serum CircZFR levels are associated with poor clinical features and prognosis in CRC patients, making it a promising biomarker for liquid biopsy.

CircZFR promotes CRC cell proliferation and motility

The expression of circZFR but not linZFR in CRC tissues and serum indicates its oncogenic property. Therefore, we detected its expression in various CRC cell lines and chose HCT116 and Colo320 which exhibited relatively higher levels of circZFR for the following experiments (Fig. 2A). We designed 4 siRNAs targeting the junction sites of circZFR and found that they did not affect linZFR expression (Fig. S2A). The sequences of si-circZFR 02 and si-circZFR 04 with higher efficiencies were used to construct shRNA

plasmids to stably knockdown circZFR (sh-circZFR in Figures refered to sh-circZFR 04). We also transfected a circZFR overexpression plasmid into HCT116 and Colo320 cells and found that it significantly enhanced the expression of circZFR but not that of linZFR (Fig. S2B). EdU and soft agar assays revealed that circZFR knockdown impaired CRC cell proliferation and circZFR overexpression promoted proliferation (Fig. 2B-C). Transwell and wound healing assays indicated that the migration and invasion abilities of CRC cells were prominently inhibited by sh-circZFR and promoted by circZFR overexpression (Fig. 2D-E and S2C-D). In addition, cell migration is a dynamic process primarily driven by the cytoskeleton, and filamentous actin (F-actin) is the vital component of cytoskeletal protein[24]. Given the effects of circZFR on cell aggressive phenotypes, we performed cytoskeleton assay and found that silencing circZFR remarkably decreased the number of F-actin in CRC cells and restrained cell migration (Fig. 2F). Following the establishment of epithelial-to mesenchymal (EMT), cancer epithelial cells acquire the mesenchymal cell traits with enhanced disseminated ability[25]. At the protein level, the expression of E-cadherin was increased and the expression of N-cadherin and matrix metallopeptidase 9 (MMP9) were decreased after circZFR knockdown, whereas circZFR overexpression had the opposite effect (Fig. 2G). Moreover, silencing circZFR augmented the apoptosis rate of CRC cells and suppressed the level of anti-apoptotic Bcl-2, whereas facilitated the expression of pro-apoptotic Bax and a series of caspase proteins (Fig. 2H-I). These data support that circZFR promotes CRC cell proliferation and motility, while silencing circZFR promotes cell apoptosis.

Exosomal circZFR is transmitted among CRC cells and promotes oncogenic phenotypes

The existence of circZFR has been found in serum exosomes of CRC patients, we then extracted exosomes from CRC cell culture medium and measured the expression of exosomal circZFR (exo-circZFR) (Fig. 2A). Interestingly, the abundance of exo-circZFR was much higher than cellular circZFR (Fig. 3B). The features of exosome derived from HCT116 and Colo320 cells were identified by TEM, DLS, and expressed marker proteins TSG101, CD63 and CD81 (Fig. 3C-E). Subsequently, we isolated exosomes from HCT116 and Colo320 cells that were transfected with the circZFR overexpression or N.C plasmids and found that exo-circZFR levels were strongly increased after circZFR overexpression (Fig. 3F). CRC cells (WT) were incubated with different concentrations of exosomes from circZFR/N.C groups for 48h and collected for EdU and Transwell assays. The results revealed that exo-circZFR dramatically promoted CRC cell proliferation and migration, which is similar to that obtained by the direct overexpression of circZFR in CRC cells. We also found that higher concentration of exo-circZFR had better enhancement of cell migration but not of proliferation (Fig. 3G-H). These data substantiate an oncogenic role of exo-circZFR in CRC development.

Silencing circZFR reduces CRC growth and inhibits pulmonary and hepatic metastasis *in vivo*

To further investigate the effect of circZFR *in vivo*, we primarily established luciferase-expression HCT116 cells transfected with N.C or sh-circZFR vectors to generate tumors in nude mice. After three weeks of subcutaneous injection, we observed that circZFR knockdown markedly suppressed tumor formation when compared with N.C group, as evidenced by *in vivo* bioluminescence imaging and *ex vivo* tumor

imaging (Fig. 4A-B). Furthermore, immunohistochemistry (IHC) staining indicated that the expression of Ki67, a typical marker of cell growth, was reduced after circZFR knockdown (Fig. 4C). To elucidate the role of circZFR in regulating CRC metastasis, we then conducted pulmonary and hepatic metastasis experiments. After four weeks of tail vein injection, bioluminescence imaging demonstrated that luciferase activity was strongly decreased in the circZFR knockdown group (Fig. 4D). *Ex vivo* imaging of lungs showed obvious metastases in the N.C group, however, tumors in the circZFR knockdown group were too small to be seen (Fig. 4E). Similarly, we found that the hepatic metastasis was strongly restrained in the circZFR knockdown group following intrasplenic injection for five weeks (Fig. 4F-G). Moreover, Haematoxylin and eosin (H&E) results showed morphological differences of metastases between different groups and IHC staining indicated that changes in the expression of E-cadherin and N-cadherin were in agreement with the *in vitro* results (Fig. 4H-I). Overall, these data suggest that silencing circZFR expression suppresses the capacity of CRC growth and metastasis *in vivo*.

ESRP1 promotes circZFR generation in CRC cells

Back-splicing of precursor mRNA (pre-mRNA) requires looping of the introns that flank the downstream and upstream exons[26]. This structure can be facilitated by inverted repeated *Alu* pairs or by dimerization of RNA-binding proteins (RBPs)[26, 27]. Dysregulation of these RBPs in cancer development can disturb the competition between canonical linear splicing and back-splicing, leading to dysregulation of circRNA expression[28, 29]. In order to gain a deeper understanding of circZFR generation, we retrieved the TCGA database and found that the expression of ESRP1, polypyrimidine tract binding protein 1 (PTBP1) and nudix-type motif 21 (NUDT21) were significantly upregulated in CRC tissues compared with matched normal tissues, which was consistent with the circZFR level (data not shown). To clarify which RBP was involved in this process, we designed two siRNAs that specifically targeted mRNAs of these RBPs and then assessed the knockdown efficiency. The expression of circZFR was further detected in HCT116 and Colo320 cell lines transfected with these siRNAs, and the results showed that only silencing ESRP1 leaded to a loss of circZFR expression (Fig. 5A-B). Furthermore, we found increased expression of linZFR but not pre-mRNA of ZFR (pre-ZFR) after ESRP1 knockdown (Fig. 5B). Clinically, the expression of ESRP1 was positively correlated with circZFR expression in tumor tissues of 40 CRC patients (Fig. 5C).

Next, we discovered five putative ESRP1-binding sequences (GGT-rich) in the upstream and downstream region of pre-ZFR and three putative sites on introns between looped exons[30, 31], and designed six pairs of primers (a-f) targeting all the putative binding sequences (Fig. 5D). RBP immunoprecipitation (RIP) presented that ESRP1 could bind to the putative sites on the flanking introns of pre-ZFR, but not the sites on the internal introns (Fig. 5E). We then investigated whether deleting the proved binding sequences could affect circZFR generation. According to CRISPR/Cas9 system, two plasmids containing respective guide RNAs (gRNA1 and gRNA2) that targeting the both sites of upstream binding sequences were designed and transfected into CRC cells simultaneously. The monoclonal cells were then selected and the deleting efficiency of circZFR was examined as shown in Fig. 4F, suggesting that the endogenous circulation of circZFR was significantly blocked. To further explore the effects of ESRP1 binding on the cell phenotypes, we co-overexpressed circZFR in CRISPR/Cas9-edited CRC cells and assessed the

expression of circZFR (Fig. 5F). EdU and Transwell assays demonstrated that deleting ESRP1 binding sequences in CRC cells suppressed their proliferation and migration, which could be rescued by circZFR overexpression (Fig. 5G-H). In conclusion, ESRP1 accelerates the biogenesis of circZFR via targeting some binding sites in flanking intronic regions in CRC cells.

CircZFR directly binds to BCLAF1 and inhibits its degradation

To explore the molecular mechanism underlying circZFR, we primarily applied RNA pulldown coupled with silver staining and MS analysis to characterize potential circZFR-binding proteins. According to MS results, we selected the top 10 RBPs that probably interacting with circZFR (Fig. 6A and S3A). Subsequently, we retrieved all these proteins in TCGA and UniProt databases as well as published references and found that BCLAF1, transferrin (TF), DEAD box polypeptide 18 (DDX18) and calpain 1 (CAPN1) were promising functional proteins in CRC development[32-35]. Thus, we performed RNA pulldown to validate the interaction between these RBPs and circZFR and the results showed that only BCLAF1 could specifically combine with circZFR (Fig. 6B and S3B, negative data not shown). RIP assay further confirmed that anti-BCLAF1 antibody pulled down abundant circZFR compared to IgG (Fig. 6C). Interestingly, ectopic expression of circZFR promoted BCLAF1 protein levels but not mRNA level, whereas knockdown inhibited the expression of BCLAF1 protein but did not decrease its mRNA level, suggesting that circZFR may regulate the stability of BCLAF1 protein at post-transcriptional level (Fig. 6D-E). In agreement with the *in vitro* results, IHC staining images showed decreased expression of BCLAF1 in the circZFR knockdown group of three mouse models (Fig. 6F). To assess this hypothesis, circZFR-overexpressing and N.C cells were treated with CHX to inhibit protein synthesis for the indicated time periods. The results showed that the degradation of BCLAF1 was remarkably retarded when circZFR was overexpressed. Moreover, the expression level of BCLAF1 protein in CRC cells cotreated with the proteasome inhibitor MG132 was markedly rescued compared to that cotreated with the lysosome inhibitor chloroquine (Fig. 6G). These findings suggested that circZFR likely suppressed BCLAF1 degradation via the ubiquitination-proteasome system. We then transfected FLAG-tagged BCLAF1 plasmid into circZFR-overexpressing/N.C HCT116 cells and detected the ubiquitination of BCLAF1. IP results revealed that BCLAF1 was less ubiquitinated in circZFR-overexpressing cells compared to N.C cells after MG132 treatment (Fig. 6H). These results indicate that circZFR interacts with BCLAF1 to restrain its ubiquitination and degradation.

Protein ubiquitination is a dynamic process and a fundamental posttranscriptional modification (PTM). Here, we focused on two types of enzymes responsible for this process including E3 ubiquitin ligases that engender ubiquitin and deubiquitinases (DUBs) that reverse ubiquitin[36, 37]. To further clarify the effect of circZFR binding on BCLAF1 ubiquitination, we treated circZFR-overexpressing/N.C CRC cells with PR619 to inhibit the function of DUBs and found that PR619 had no significant effect on the expression of BCLAF1 in different cell groups, suggesting that circZFR may not act as a protein scaffold to facilitate colocalization of BCLAF1 and its specific DUB (Fig. 6I). Therefore, we speculated that the pattern of circZFR-BCLAF1 interaction was likely to be protein sponge, in which circZFR and specific E3 ubiquitin ligase with shared BCLAF1 binding sites competed for binding with BCLAF1. CircZFR directly interacted

with BCLAF1 and acted to prevent E3-induced BCLAF1 degradation. However, the specific E3 ligase of BCLAF1 need further exploration. Zhou et al. observed that BCLAF1 increased colon cell growth, whereas had no significant effect on cell apoptosis[35]. Here, we designed two siRNAs targeting BCLAF1 and assessed the knockdown efficiency (Fig. S3C). CCK8 and Transwell assays showed that silencing BCLAF1 suppressed CRC cell proliferation and migration (Fig. S3D-E). However, it seemed unlikely that BCLAF1 acted as an apoptosis inducer according to the cell cytometry results (Fig. S3F). Moreover, the decreased proliferation and migration of CRC cells caused by circZFR knockdown could be partly rescued by co-overexpressing BCLAF1 (Fig. 6J-K). The efficiency of BCLAF1 overexpression was demonstrated in Fig. S3G. Based on these data, circZFR binds to BCLAF1 and inhibits its E3-ligase mediated ubiquitination and degradation, thereby facilitating CRC growth and metastasis.

CircZFR serves as a sponge for CRC suppressive miR-3127-5p

Given that the interaction of circZFR and BCLAF1 is not responsible for increased cell apoptosis caused by circZFR knockdown, we investigated whether circZFR could mediate CRC cell apoptosis via other mechanism of action. CircRNAs located in the cytoplasm can influence cancer development through binding and sequestration of miRs[38]. Moreover, we identified circZFR from ceRNA microarray, reminding us to further clarify the miR sponge theory. We firstly predicted the potential interactions between circZFR and miRs through four databases including circBank, miRanda, RNAhybrid and Targetscan. The expression abundance of the overlapped miRs was then analyzed by TCGA database. Here, we focused on five miRs with relatively high abundance and were down-regulated in CRC tissues compared to normal tissues for further investigation (Fig. 7A and S4A). Secondly, the complete circZFR sequence was inserted into the downstream of the dual-luciferase reporter gene to construct the luciferase reporter vector. The vector was co-transfected with miR mimics into 293T cells and the result demonstrated that both the miR-1266-5p and miR-3127-5p mimics caused about 40% inhibition of luciferase activity compared with the miR-NC group, suggesting the direct interaction between these two miRs and circZFR (Fig. 7B). Since Argonaute 2 (AGO2) is a key component in miR sponging events, we then retrieved circInteractome and identified potential AGO2-binding sites within circZFR sequence that based on crosslinking-immunoprecipitation (CLIP) data set. Further RIP experiment validated the interaction between circZFR and AGO-2 protein in HCT116 cells (Fig. 7C). Next, CCK-8, migration and flow cytometry assays were performed to investigate if these two miR candidates were functional in CRC. The results showed that excess miR-3127-5p was more significant in inhibiting cell proliferation than miR-1266-5p, and could greatly restrain cell migration and promoted apoptosis. However, miR-1266-5p had no effect on migration and apoptosis (Fig. S4B-D).

Subsequent Western blotting demonstrated that changes in the expression of the EMT and apoptotic markers were also in agreement with altered cellular behavior by miR overexpression (Fig. 7D). Moreover, FISH assay confirmed the co-localization of circZFR and miR-3127-5p in cytoplasm of HCT116 and Colo320, which was a prerequisite for a sponging function (Fig. 7E). We further found a potential binding sequence between circZFR and miR-3127-5p and constructed a circZFR luciferase reporter vector with mutant-type sequences (MUT). Next, circZFR-WT or MUT was cotransfected with miR-NC or miR-3127-5p

mimic. Results showed that the relative luciferase activity was lower in CRC cells transfected with WT vectors while no significant difference was observed in the MUT group (Fig. 7F). To confirm whether circZFR affected CRC progression through miR-3127-5p, we transfected miR mimics alone or together with the circZFR overexpression plasmid in CRC cells. CCK-8 and Transwell assays showed that circZFR overexpression was able to partly reverse the inhibitory impacts of miR-3127-5p upregulation on cell proliferation and motility (Fig. 7G-H). Therefore, we speculated that circZFR may exert oncogenic functions by sponging CRC suppressive miR-3127-5p.

MiR-3127-5p targets RTKN2 to regulate oncogenic phenotypes including apoptosis of CRC cells

Since circRNA can positively regulate target mRNA translation through sequestering miR, we performed RNA-seq in HCT116 cells that stably transfected with N.C or sh-circZFR plasmid and focused on the weakly expressed genes in the sh-circZFR group compared to N.C. group. The heatmap of differentially expressed genes was shown in Fig. S5A. Then we retrieved two online databases to predict the potential target mRNAs containing complementary nucleotide sequences of miR-3127-5p and found ten genes from the intersection of the three (Fig. 8A). Among them, RTKN2, LFNG O-fucosylpeptide 3-beta-N-acetylglucosaminyltransferase (LFNG) and hepatocyte nuclear factor 4 alpha (HNF4A) were remarkably upregulated in CRC tissues compared to normal tissues from TCGA database (Fig. S5B). After qRT-PCR validation, we found that circZFR-deficient CRC cells exhibited decreased RTKN2 level, whereas circZFR overexpression facilitated the expression of RTKN2 (Fig. 8B and S5C). Pang and colleagues found that RTKN2 had oncogenic activity in colon cancer and silencing RTKN2 could induce cell apoptosis[39]. Here, we validated the effect of RTKN2 on apoptosis of CRC cells transfected with N.C or RTKN2 siRNAs, and results was consistent with the reported literatures (Fig. S5D-E). Moreover, IHC staining images in three mouse models revealed that the expression of RTKN2 was strongly downregulated in circZFR knockdown group (Fig. 8C). We then inserted the luciferase reporter with WT or MUT binding sequences in RTKN2 3'-UTR to validate the interaction of miR-3127-5p and RTKN2. Results from dual-luciferase reporter assay revealed that RTKN2 could be the target of miR-3127-5p (Fig. 8D). Furthermore, the expression of circZFR was positively correlated to the mRNA level of RTKN2 in 40 tumor tissues of primary CRC patients (Fig. 8E). To further confirm whether RTKN2 is the direct target of the circZFR/miR-312705p axis, we performed western blotting and found that silence of circZFR suppressed the level of RTKN2 and this decreased RTKN2 expression was reversed by miR-3127-5p inhibitor (Fig. 8F). Similarly, circZFR overexpression increased the level of RTKN2, which was recovered by miR-3127-5p mimic (Fig. 8G). Our previous data confirmed that circZFR was not likely to regulate apoptosis of CRC cells through binding to BCLAF1, therefore, whether the miR-3127-5p/RTKN2 axis contributes to circZFR-induced apoptosis alteration was analyzed. Results showed that the decreased expression of Bcl-2 caused by circZFR deficiency was reversed by co-overexpressing RTKN2 and the enhanced expression of Bax and caspase proteins after circZFR knockdown was repressed by co-overexpression of RTKN2 (Fig. 8H). The efficiency of RTKN2 overexpressing plasmid was assessed and shown in Fig. S5F. Interestingly, we found that increasing BCLAF1 and RTKN2 levels simultaneously in CRC cells transfected with sh-circZFR vector could reverse the effect of circZFR knockdown on the expression of metastasis-related markers (Fig. 8I).

Anti-cancer efficacy of TCP1-CD-QDs loaded with si-circZFR in CRC cells and PDX models

The above results verified that circZFR exhibited significant oncogenic effects on CRC progression and metastasis, making it a promising anti-cancer target. In view of the limitations of RNA interference (RNAi)-based strategy including inefficient intracellular delivery resulting from nuclease degradation and potential adverse effects caused by delivery to off-target tissues or cells[9, 40], we attempted to optimize the si-circZFR delivery system. It has been reported that NPs with high loading efficiency and biological safety are capable of drug and small nucleic acid delivery[41-44]. Moreover, our group designed a novel TCP1-CD-QDs nanocarrier and verified its loading capacity of chemotherapeutic drug 5-Fu and nucleotide drug miR-34a in CRC therapy[21]. Therefore, we firstly evaluated the effect of TCP1-CD-QD NPs on cellular uptake. As shown in Fig. 9A, red fluorescence was observed in HCT116 and Colo320 cells incubated with the NPs. Subsequently, si-circZFR 04 (referred to as si-circZFR hereafter) was loaded into TCP1-CD-QDs by self-assembly with CD and incubated with CRC cells. The knockdown efficiency of circZFR in this system was more than 50%, whereas the linZFR level was not affected (Fig. 9B). Compared to cells incubated with N.C siRNA and TCP1-CD-QDs, delivering si-circZFR via TCP1-CD-QDs nanocarrier could significantly inhibit proliferation and motility of CRC cells (Fig. 9C-E, S6A-B).

In the following experiments, we collected CRC tissues from a stage □ patient and constructed PDX models to better assess the intricate *in vivo* NP performance. The level of circZFR in tumor tissue of this CRC patient was higher than the adjacent normal tissues, which was detected in Fig. 1B. Fifteen PDX mice were randomly divided into three groups and intravenously injected with PBS, Chol-conjugated si-circZFR or TCP1-CD-QDs loaded with si-circZFR (referred to as PBS group, si-circZFR group and nanocarrier group) every three days. Notably, conjugation of Chol is responsible for the stability of single si-circZFR in circulation system. As a result, we found an effective reduction of the tumor volume and tumor weight in both the si-circZFR group and nanocarrier group relative to PBS group. Particularly, treatment with TCP1-CD-QDs loaded with si-circZFR resulted in a stronger suppressive effect of CRC growth compared to that with Chol-conjugated si-circZFR (Fig. 9F). Further H&E staining of the tumors in each group indicated that the tissue differentiation in PBS group was poor. However, circZFR knockdown in other two groups remarkably improved tissue differentiation, especially in the nanocarrier group, as exemplified by the morphology of intestinal epithelium (Fig 9G). We detected the expression levels of Ki67, BCLAF1 and RTKN2 in each group and found lower expression of these proteins in si-circZFR and nanocarrier groups, which was consistent with the results reported in CRC cell-derived xenograft models (Fig. 9H). Finally, to investigate the biosafety of NP delivery, we examined the levels of typical serum indicators that related to liver and kidney functions[45]. As shown in Fig. S6C-D, the levels of alanine aminotransferase (ALT), aspartate aminotransferase (AST), creatinine (CRE) and blood urea nitrogen (BUN) were of no significant difference. Further H&E staining images of the major organs showed that there were no obvious pathological changes of heart, lung, liver, kidney and spleen in each group (Fig. S6E). These results suggested that TCP1-CD-QDs can deliver si-circZFR to CRC cells and inhibit aggressive phenotypes. Moreover, the use of TCP1-CD-QDs loaded with si-circZFR can achieve better suppressive effect on tumor growth and stronger promoting effect on tumor differentiation *in vivo* than single si-circZFR. This NP delivery system with undetectable side effects could be a very attractive

direction for anti-tumor therapy based on circZFR. Altogether, the schematic diagram of the mechanisms of circZFR in CRC progression was shown in Fig 9I.

Discussion

Dysregulated circRNAs that contribute to cancer development always show tissue-specific even cell type-specific expression patterns[46, 47]. Moreover, the unique looping structure of circRNAs rendering them extremely stable due to exonuclease resistance[48]. These characteristics imply the strong biomarker potential of these molecules. To date, emerging studies have detected dysregulated individual circRNAs or circRNA panels not only in tissues and cells but also in body fluids (including serum, plasma, urine, and gastric juice) across pan-cancers[49], suggesting their diagnostic and prognostic values as non-invasive biomarkers in clinical applications. The detection of circZFR in our study was conducted in both tissue and serum samples, and much higher levels of circZFR was detected in serums compared to tissues because of the exosomal export and accumulation in blood circulation. The ROC curve with AUC further substantiated the value of circZFR as a relatively non-invasive liquid biopsy marker for CRC diagnosis. However, most studies reported the biomarker potential of individual circRNAs with limited validation and retrospective studies. Thus, individual circRNA or circRNA signatures could potentially be supplements to the traditional diagnostic or prognostic biomarkers if further properly validated in larger clinical samples and prospective studies.

The interplay between circRNAs and RBPs is highly complex. RBPs can regulate circRNA generation by binding to intronic regions in a cell type-specific manner[50]. In this study, we found that ESRP1 depletion disturb the balance between canonical linear pre-ZFR splicing and back-splicing that generates circZFR, suggesting that dysregulated RBPs in cancers can be one of the factors influencing the competition between these two types of splicing[51]. In addition, circRNAs can interact with RBPs and act as protein sponge[52, 53], protein scaffolds[54, 55], protein function enhancers[56] or protein recruiters[57, 58]. The first example of the protein sponge function was provided by the circRNA derived from MBNL1. The introns flanking circMbl harbored many MBL (MBNL1-encoded protein) binding sites, which facilitated the looping of circMbl. Moreover, direct interaction was found between circMbl itself and MBL protein. Therefore, overexpressed MBL decreased the production of its own mRNA but increased circMbl expression. This circRNA could in turn bind to and sponged MBL to repress its level[51]. Other two typical reports also described the competition between a circRNA and another nucleic acid for the same binding site on RBP. One study found that circPABPN1 can compete with the nuclear poly(A) binding protein 1 (PABPN1) mRNA for binding the RBP Hu-antigen R (HUR) in cervical cancer, leading to the suppression of PABPN1 translation[52]; results from another study showed that circANRIL bound to pescadillo homologue 1 (PES1), thereby occupying pre-rRNA (ribosomal RNA) binding sites at PES1 and inhibiting rRNA maturation[53].Interestingly, many individual circRNAs have been shown to compete with another protein for RBP binding sites. Yang et al. found that circPTK2 interacted with vimentin at its phosphorylation sites Ser38, Ser55 and Ser82, impairing the binding of phosphorylases and inhibiting the solubility of vimentin[59]. Another example has been provided by Shen et al., who showed that circECE1 interacted with c-Myc to prevent its degradation by speckle-type POZ (SPOP), the specific E3 ubiquitin

ligase of c-Myc. The results indicated that the SPOP binding motifs overlapped with the circECE1 binding site, excess circECE1 promoted c-Myc expression by restraining the SPOP-mediated ubiquitination[60]. Like c-Myc, BCLAF1 is an onco-protein involved in CRC progression that leads to increased cell proliferation[35]. Intriguingly, our study suggested that circZFR may compete with a specific E3 ligase for the same binding site on BCLAF1 and prevent E3-mediated degradation. How circRNAs mechanistically control RBP function and homeostasis awaits further investigation.

The miRNA sponging properties of circRNAs have been extensively studied in recent years, especially in a cancer context. However, several controversies have recently emerged in this field[61]. Most of the published articles describing circRNAs that function as ceRNAs only contain a single or few binding sites for individual miRs, however, circRNAs indeed function as miR sponge may need multiple binding sites as ciRS-7 which harbors over 60 target sites for miR-7[62]. Furthermore, the abundance of many circRNAs is far less than that of miR targets and is not adequate to sequester enough miRs[38]. In our study, the results of correlation analysis suggested that circZFR has similar abundance with RTKN2, and the ratio is equal between the RTKN2 miR response elements (MREs) and MREs in circZFR, providing additional evidence for the sponging function. On the other hand, recent study found that the correlations between the expression levels of circRNAs, miRs, and the miR targets are more likely to derive from co-expression or mutual exclusivity within diverse subpopulations of cells in complex cancer tissues[63]. Therefore, stronger experimental evidences are needed to support the sponging function. In the present study, co-localization experiment is a prerequisite for sponging, luciferase reporter assay and RIP assay provide direct evidence for the interaction of circZFR and miR-3127-5p, further functional studies imply potential validation of the circ-miR axis. To gain a deeper understanding about the pitfalls surrounding the miR sponging function of circRNAs can facilitate more thorough investigations in future studies.

Lastly, circRNAs might also be used as promising targets for anticancer therapy given their abundant functional roles in cancer progression. To date, the common approach to inhibit or degrade oncogenic circRNAs is RNAi-based strategies and most loss-of-function studies are typically performed using RNAi (including siRNA or shRNA) for circRNA knockdown. However, there are some limitations of RNAi molecules during clinical application[40]. Nanotechnologies have attracted remarkable interest in the field of cancer research since their distinctive features for imaging, diagnosis and the delivery of drugs or/and therapeutic agents[64]. The use of NPs may overcome the limitations of RNAi molecules because they can increase the permeation and retention of carried siRNAs in the circulatory system, deliver them specifically to target sites, and prevent immune activation[65]. Our research used TCP1-CD-QDs as a delivery carrier of si-circZFR in PDX models and the results showed that this delivery system could efficiently target CRC sites with lower dose than siRNAs and undetectable side effects. Nanomedicines incorporating new therapeutic agent like siRNA have prospective roles in cancer treatment, whereas some challenges must be addressed begore their full impacts can be realized. Improving the techniques of controlled and scalable NP synthesis as well as developing novel animal models that closely reproduce the heterogeneity of human tumors will facilitate the transition of safer and more effective nanomedicines from laboratory to clinic[64]. Similar to NP delivery, exosomes can also carry RNAi molecules to targeted tissues in a safe and efficient way[66, 67]. The unique membrane protein and lipid

composition prevent exosomes from degradation and improve their cellular uptake, which is not found in synthetic NPs[68]. However, exosomes face their own challenges in scalable manufacturing and particle heterogeneity[67, 69]. With many innovative technologies under development for both synthetic NP and exosome delivery, technical issues in the circRNA targeting will be addressed in the foreseeable future to bring circRNAs to the forefront of clinical therapy.

Conclusions

In summary, our study is the first to identify circZFR as a novel biomarker especially for liquid biopsy in CRC diagnosis. CircZFR exerts its oncogenic effects by interacting with BCLAF1 to restrain its degradation and regulating the miR-3127-5p/RTKN2 axis. We also demonstrate an effective approach to inhibiting CRC growth by TCP1-CD-QDs-siRNA complex targeting circZFR. These observations helped elucidate the progression of CRC and suggest that the combination of NPs and circRNAs holds promise as a new therapeutic strategy.

Abbreviations

CRC
colorectal cancer
circRNA
circular RNA
ceRNA
competing endogenous RNA
TMA
tissue microarray
FISH
fluorescence in situ hybridization
ZFR
zinc finger RNA binding protein
qRT-PCR
quantitative real-time polymerase chain reaction
RIP
RNA immunoprecipitation
ESRP1
epithelial splicing regulatory protein 1
BCLAF1
BCL2-associated transcription factor 1
RTKN2
rhotekin 2
TME

tumor microenvironment
TNM
tumor, node, metastasis
IHC
immunohistochemistry
RNAi
RNA interference
PDX
patient-derived xenograft

Declarations

Acknowledgements

Not applicable.

Author's contributions

Zhangfa Song conceived of the study and carried out its design. Jiaxin Chen, Jianbin Xu and Huijuan Wang performed the experiments. Engeng Chen, Qing Meng and Jiawei Wang conducted the statistical analyses. Wei Zhou and Zhenyu Ju wrote and revised the paper. All authors read and approved the final manuscript.

Funding

This study was supported by the National Natural Science Foundation of China (No.81771502, 32071349, 81701820), the Natural Science Foundation of Zhejiang Province (No. LH19H160001, LY20H180014) and the Department of Health of Zhejiang Province (No. 2018KY473 and 2018PY025).

Availability of data and materials

The ceRNA microarray and RNA-seq data analyzed during the current study are available from the corresponding author on reasonable request.

Ethics approval and consent to participate

The present study was approved by the Ethics Committee of Sir Run Run Shaw Hospital.

Consent for publication

All authors have agreed to publish this manuscript.

Competing Interest

Conflict of interest relevant to this article was not reported.

Author details

1. Department of Colorectal Surgery, Sir Run Run Shaw Hospital, Zhejiang University School of Medicine, Zhejiang, China
2. Key Laboratory of Biological Treatment of Zhejiang Province, Zhejiang, China
3. Department of Pulmonary and Critical Care Medicine, Regional medical center for National Institute of Respiratory Disease, Sir Run Run Shaw Hospital, Zhejiang University School of Medicine, Zhejiang, China
4. Key Laboratory of Regenerative Medicine of Ministry of Education, Institute of Aging and Regenerative Medicine, Jinan University, Guangzhou, China

References

1. Sung H, Ferlay J, Siegel RL, Laversanne M, Soerjomataram I, Jemal A, et al. Global Cancer Statistics 2020: GLOBOCAN Estimates of Incidence and Mortality Worldwide for 36 Cancers in 185 Countries. CA Cancer J Clin. 2021;71(3):209–49.
2. Li J, Ma X, Chakravarti D, Shalapour S, DePinho RA. Genetic and biological hallmarks of colorectal cancer. Genes Dev. 2021;35(11–12):787–820.
3. Kanth P, Inadomi JM. Screening and prevention of colorectal cancer. BMJ. 2021;374:n1855.
4. Dekker E, Tanis PJ, Vleugels JLA, Kasi PM, Wallace MB. Colorectal cancer. The Lancet. 2019;394(10207):1467–80.
5. Wu F, Yang J, Liu J, Wang Y, Mu J, Zeng Q, et al. Signaling pathways in cancer-associated fibroblasts and targeted therapy for cancer. Signal Transduct Target Ther. 2021;6(1):218.
6. Yan L, Chen YG. Circular RNAs in Immune Response and Viral Infection. Trends Biochem Sci. 2020;45(12):1022–34.
7. Chen LL. The expanding regulatory mechanisms and cellular functions of circular RNAs. Nat Rev Mol Cell Biol. 2020;21(8):475–90.
8. Kristensen LS, Andersen MS, Stagsted LVW, Ebbesen KK, Hansen TB, Kjems J. The biogenesis, biology and characterization of circular RNAs. Nat Rev Genet. 2019;20(11):675–91.
9. Singh S, Narang AS, Mahato RI. Subcellular fate and off-target effects of siRNA, shRNA, and miRNA. Pharm Res. 2011;28(12):2996–3015.
10. Yu YZ, Lv DJ, Wang C, Song XL, Xie T, Wang T, et al. Hsa_circ_0003258 promotes prostate cancer metastasis by complexing with IGF2BP3 and sponging miR-653-5p. Mol Cancer. 2022;21(1):12.
11. Qiu S, Li B, Xia Y, Xuan Z, Li Z, Xie L, et al. CircTHBS1 drives gastric cancer progression by increasing INHBA mRNA expression and stability in a ceRNA- and RBP-dependent manner. Cell Death Dis. 2022;13(3):266.

12. Xia Y, Lv J, Jiang T, Li B, Li Y, He Z, et al. CircFAM73A promotes the cancer stem cell-like properties of gastric cancer through the miR-490-3p/HMGA2 positive feedback loop and HNRNPK-mediated beta-catenin stabilization. J Exp Clin Cancer Res. 2021;40(1):103.
13. Li J, Gao X, Zhang Z, Lai Y, Lin X, Lin B, et al. CircCD44 plays oncogenic roles in triple-negative breast cancer by modulating the miR-502-5p/KRAS and IGF2BP2/Myc axes. Mol Cancer. 2021;20(1):138.
14. Xie M, Yu T, Jing X, Ma L, Fan Y, Yang F, et al. Exosomal circSHKBP1 promotes gastric cancer progression via regulating the miR-582-3p/HUR/VEGF axis and suppressing HSP90 degradation. Mol Cancer. 2020;19(1):112.
15. Chen Q, Mang G, Wu J, Sun P, Li T, Zhang H, et al. Circular RNA circSnx5 Controls Immunogenicity of Dendritic Cells through the miR-544/SOCS1 Axis and PU.1 Activity Regulation. Mol Ther. 2020;28(11):2503–18.
16. Li Y, Zheng Q, Bao C, Li S, Guo W, Zhao J, et al. Circular RNA is enriched and stable in exosomes: a promising biomarker for cancer diagnosis. Cell Res. 2015;25(8):981–4.
17. Liang G, Yang Y, Niu G, Tang Z, Li K. Genome-wide profiling of Sus scrofa circular RNAs across nine organs and three developmental stages. DNA Res. 2017;24(5):523–35.
18. Hu W, Liu C, Bi ZY, Zhou Q, Zhang H, Li LL, et al. Comprehensive landscape of extracellular vesicle-derived RNAs in cancer initiation, progression, metastasis and cancer immunology. Mol Cancer. 2020;19(1):102.
19. Wang Y, Liu J, Ma J, Sun T, Zhou Q, Wang W, et al. Exosomal circRNAs: biogenesis, effect and application in human diseases. Mol Cancer. 2019;18(1):116.
20. Santer L, Bär C, Thum T. Circular RNAs: A Novel Class of Functional RNA Molecules with a Therapeutic Perspective. Mol Ther. 2019;27(8):1350–63.
21. Xu J, Zhang G, Luo X, Wang D, Zhou W, Zhang Y, et al. Co-delivery of 5-fluorouracil and miRNA-34a mimics by host-guest self-assembly nanocarriers for efficacious targeted therapy in colorectal cancer patient-derived tumor xenografts. Theranostics. 2021;11(5):2475–89.
22. Chen J, Wu Y, Luo X, Jin D, Zhou W, Ju Z, et al. Circular RNA circRHOBTB3 represses metastasis by regulating the HuR-mediated mRNA stability of PTBP1 in colorectal cancer. Theranostics. 2021;11(15):7507–26.
23. Merlino G, Miodini P, Callari M, D'Aiuto F, Cappelletti V, Daidone MG. Prognostic and functional role of subtype-specific tumor-stroma interaction in breast cancer. Mol Oncol. 2017;11(10):1399–412.
24. Seetharaman S, Etienne-Manneville S. Cytoskeletal Crosstalk in Cell Migration. Trends Cell Biol. 2020;30(9):720–35.
25. Zhang N, Ng AS, Cai S, Li Q, Yang L, Kerr D. Novel therapeutic strategies: targeting epithelial–mesenchymal transition in colorectal cancer. The Lancet Oncology. 2021;22(8):e358-e68.
26. Xiao MS, Ai Y, Wilusz JE. Biogenesis and Functions of Circular RNAs Come into Focus. Trends Cell Biol. 2020.

27. Zhang XO, Wang HB, Zhang Y, Lu X, Chen LL, Yang L. Complementary sequence-mediated exon circularization. Cell. 2014;159(1):134–47.
28. Vo JN, Cieslik M, Zhang Y, Shukla S, Xiao L, Zhang Y, et al. The Landscape of Circular RNA in Cancer. Cell. 2019;176(4):869–81 e13.
29. Conn SJ, Pillman KA, Toubia J, Conn VM, Salmanidis M, Phillips CA, et al. The RNA binding protein quaking regulates formation of circRNAs. Cell. 2015;160(6):1125–34.
30. Zhao W, Cui Y, Liu L, Qi X, Liu J, Ma S, et al. Splicing factor derived circular RNA circUHRF1 accelerates oral squamous cell carcinoma tumorigenesis via feedback loop. Cell Death Differ. 2020;27(3):919–33.
31. Zeng K, He B, Yang BB, Xu T, Chen X, Xu M, et al. The pro-metastasis effect of circANKS1B in breast cancer. Mol Cancer. 2018;17(1):160.
32. Zheng S, Hu L, Song Q, Shan Y, Yin G, Zhu H, et al. miR-545 promotes colorectal cancer by inhibiting transferring in the non-normal ferroptosis signaling. Aging (Albany NY). 2021;13(24):26137–47.
33. Wang P, Zheng H, Zhang J, Wang Y, Liu P, Xuan X, et al. Identification of key gene modules and genes in colorectal cancer by co-expression analysis weighted gene co-expression network analysis. Biosci Rep. 2020;40(9).
34. Chen J, Wu Y, Zhang L, Fang X, Hu X. Evidence for calpains in cancer metastasis. J Cell Physiol. 2019;234(6):8233–40.
35. Zhou X, Li X, Cheng Y, Wu W, Xie Z, Xi Q, et al. BCLAF1 and its splicing regulator SRSF10 regulate the tumorigenic potential of colon cancer cells. Nat Commun. 2014;5:4581.
36. Strieter ER, Korasick DA. Unraveling the complexity of ubiquitin signaling. ACS Chem Biol. 2012;7(1):52–63.
37. Komander D. The emerging complexity of protein ubiquitination. Biochem Soc Trans. 2009;37(Pt 5):937–53.
38. Jarlstad Olesen MT, L SK. Circular RNAs as microRNA sponges: evidence and controversies. Essays Biochem. 2021;65(4):685–96.
39. Pang X, Li R, Shi D, Pan X, Ma C, Zhang G, et al. Knockdown of Rhotekin 2 expression suppresses proliferation and induces apoptosis in colon cancer cells. Oncol Lett. 2017;14(6):8028–34.
40. He AT, Liu J, Li F, Yang BB. Targeting circular RNAs as a therapeutic approach: current strategies and challenges. Signal Transduct Target Ther. 2021;6(1):185.
41. Bertrand N, Wu J, Xu X, Kamaly N, Farokhzad OC. Cancer nanotechnology: the impact of passive and active targeting in the era of modern cancer biology. Adv Drug Deliv Rev. 2014;66:2–25.
42. Chen D, Love KT, Chen Y, Eltoukhy AA, Kastrup C, Sahay G, et al. Rapid discovery of potent siRNA-containing lipid nanoparticles enabled by controlled microfluidic formulation. J Am Chem Soc. 2012;134(16):6948–51.
43. Garbayo E, Pascual-Gil S, Rodriguez-Nogales C, Saludas L, Estella-Hermoso de Mendoza A, Blanco-Prieto MJ. Nanomedicine and drug delivery systems in cancer and regenerative medicine. Wiley

Interdiscip Rev Nanomed Nanobiotechnol. 2020;12(5):e1637.

44. van der Meel R, Sulheim E, Shi Y, Kiessling F, Mulder WJM, Lammers T. Smart cancer nanomedicine. Nat Nanotechnol. 2019;14(11):1007–17.
45. Moore L, Yang J, Lan TT, Osawa E, Lee DK, Johnson WD, et al. Biocompatibility Assessment of Detonation Nanodiamond in Non-Human Primates and Rats Using Histological, Hematologic, and Urine Analysis. ACS Nano. 2016;10(8):7385–400.
46. Lorenzi L, Chiu HS, Avila Cobos F, Gross S, Volders PJ, Cannoodt R, et al. The RNA Atlas expands the catalog of human non-coding RNAs. Nat Biotechnol. 2021;39(11):1453–65.
47. Ruan H, Xiang Y, Ko J, Li S, Jing Y, Zhu X, et al. Comprehensive characterization of circular RNAs in ~ 1000 human cancer cell lines. Genome Med. 2019;11(1):55.
48. Kristensen LS, Jakobsen T, Hager H, Kjems J. The emerging roles of circRNAs in cancer and oncology. Nat Rev Clin Oncol. 2021.
49. Wang S, Zhang K, Tan S, Xin J, Yuan Q, Xu H, et al. Circular RNAs in body fluids as cancer biomarkers: the new frontier of liquid biopsies. Mol Cancer. 2021;20(1):13.
50. Okholm TLH, Sathe S, Park SS, Kamstrup AB, Rasmussen AM, Shankar A, et al. Transcriptome-wide profiles of circular RNA and RNA-binding protein interactions reveal effects on circular RNA biogenesis and cancer pathway expression. Genome Med. 2020;12(1):112.
51. Ashwal-Fluss R, Meyer M, Pamudurti NR, Ivanov A, Bartok O, Hanan M, et al. circRNA biogenesis competes with pre-mRNA splicing. Mol Cell. 2014;56(1):55–66.
52. Abdelmohsen K, Panda AC, Munk R, Grammatikakis I, Dudekula DB, De S, et al. Identification of HuR target circular RNAs uncovers suppression of PABPN1 translation by CircPABPN1. RNA Biol. 2017;14(3):361–9.
53. Holdt LM, Stahringer A, Sass K, Pichler G, Kulak NA, Wilfert W, et al. Circular non-coding RNA ANRIL modulates ribosomal RNA maturation and atherosclerosis in humans. Nat Commun. 2016;7:12429.
54. Du WW, Fang L, Yang W, Wu N, Awan FM, Yang Z, et al. Induction of tumor apoptosis through a circular RNA enhancing Foxo3 activity. Cell death and differentiation. 2017;24(2):357–70.
55. Du WW, Yang W, Liu E, Yang Z, Dhaliwal P, Yang BB. Foxo3 circular RNA retards cell cycle progression via forming ternary complexes with p21 and CDK2. Nucleic Acids Res. 2016;44(6):2846–58.
56. Chen RX, Chen X, Xia LP, Zhang JX, Pan ZZ, Ma XD, et al. N(6)-methyladenosine modification of circNSUN2 facilitates cytoplasmic export and stabilizes HMGA2 to promote colorectal liver metastasis. Nat Commun. 2019;10(1):4695.
57. Chen N, Zhao G, Yan X, Lv Z, Yin H, Zhang S, et al. A novel FLI1 exonic circular RNA promotes metastasis in breast cancer by coordinately regulating TET1 and DNMT1. Genome Biol. 2018;19(1):218.
58. Wang L, Long H, Zheng Q, Bo X, Xiao X, Li B. Circular RNA circRHOT1 promotes hepatocellular carcinoma progression by initiation of NR2F6 expression. Mol Cancer. 2019;18(1):119.

59. Yang H, Li X, Meng Q, Sun H, Wu S, Hu W, et al. CircPTK2 (hsa_circ_0005273) as a novel therapeutic target for metastatic colorectal cancer. Molecular cancer. 2020;19(1):13.
60. Shen S, Yao T, Xu Y, Zhang D, Fan S, Ma J. CircECE1 activates energy metabolism in osteosarcoma by stabilizing c-Myc. Molecular cancer. 2020;19(1):151.
61. Li HM, Ma XL, Li HG. Intriguing circles: Conflicts and controversies in circular RNA research. Wiley Interdiscip Rev RNA. 2019;10(5):e1538.
62. Hansen TB, Jensen TI, Clausen BH, Bramsen JB, Finsen B, Damgaard CK, et al. Natural RNA circles function as efficient microRNA sponges. Nature. 2013;495(7441):384–8.
63. Kristensen LS, Ebbesen KK, Sokol M, Jakobsen T, Korsgaard U, Eriksen AC, et al. Spatial expression analyses of the putative oncogene ciRS-7 in cancer reshape the microRNA sponge theory. Nat Commun. 2020;11(1):4551.
64. Shi J, Kantoff PW, Wooster R, Farokhzad OC. Cancer nanomedicine: progress, challenges and opportunities. Nat Rev Cancer. 2017;17(1):20–37.
65. Ma X, Zhao Y, Liang XJ. Theranostic nanoparticles engineered for clinic and pharmaceutics. Acc Chem Res. 2011;44(10):1114–22.
66. Kamerkar S, LeBleu VS, Sugimoto H, Yang S, Ruivo CF, Melo SA, et al. Exosomes facilitate therapeutic targeting of oncogenic KRAS in pancreatic cancer. Nature. 2017;546(7659):498–503.
67. Ferguson SW, Nguyen J. Exosomes as therapeutics: The implications of molecular composition and exosomal heterogeneity. J Control Release. 2016;228:179–90.
68. El-Andaloussi S, Lee Y, Lakhal-Littleton S, Li J, Seow Y, Gardiner C, et al. Exosome-mediated delivery of siRNA in vitro and in vivo. Nat Protoc. 2012;7(12):2112–26.
69. Setten RL, Rossi JJ, Han SP. The current state and future directions of RNAi-based therapeutics. Nat Rev Drug Discov. 2019;18(6):421–46.

Tables

Table 1 is available in the Supplementary Files section.

Figures

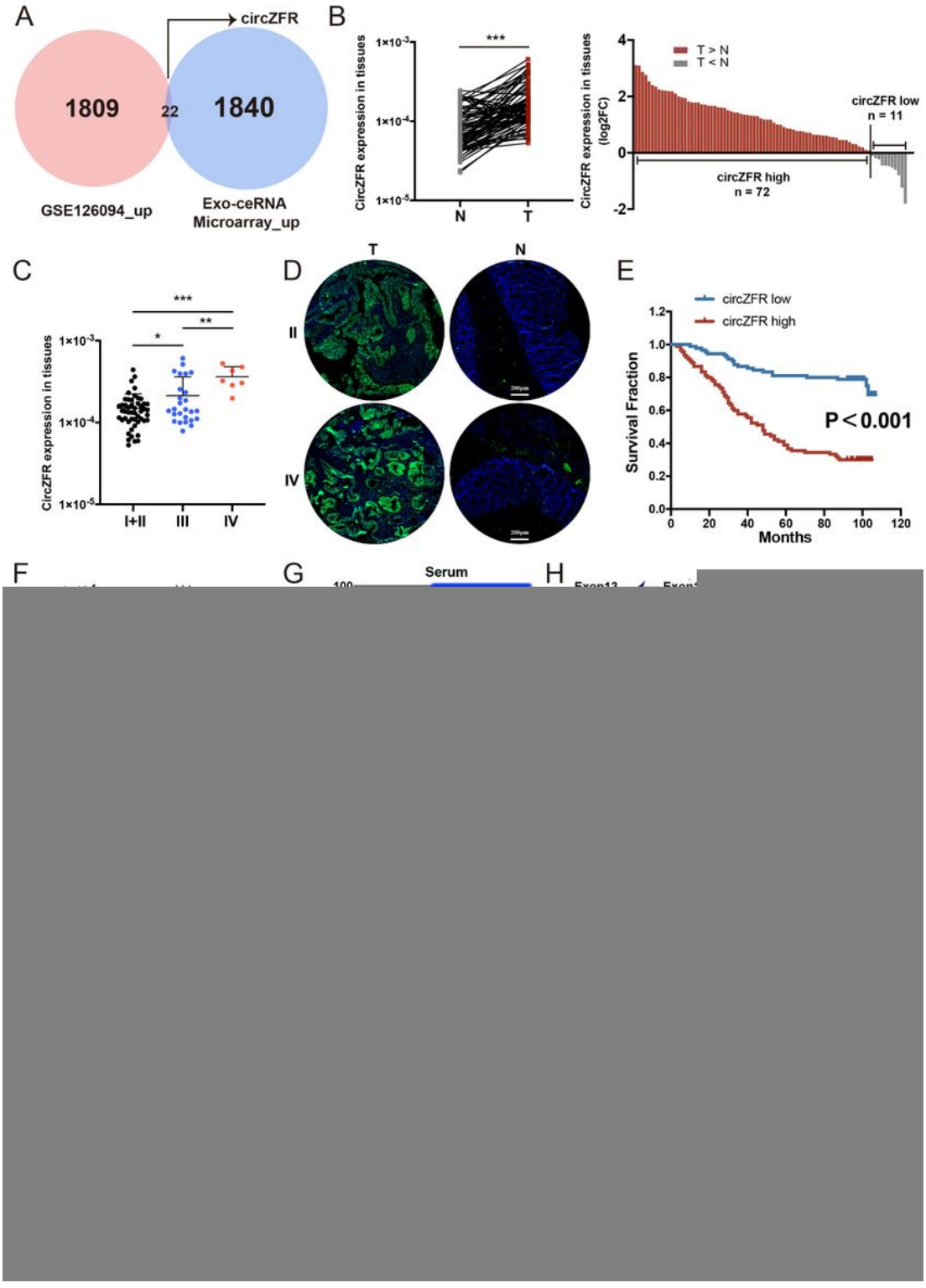

Figure 1

Expression validation and characterization of circZFR in CRC tissues and serum. A Venn diagram demonstrating the overlap of circRNAs that both elevated in CRC tissues from GSE126094 and m-CRCs' serum exosomes from ceRNA microarray. **B** Levels of circZFR in 83 pairs of CRC and matched normal tissues, as detected by qRT-PCR. (Cases: upregulated vs. downregulated = 72 vs. 11). The p values were determined by paired Student's t-tests. **C** Levels of circZFR in 83 cancer tissues of different TNM stages,

as detected by qRT-PCR. The p values were determined by one-way ANOVA. **D** Representative fluorescence images of circZFR in stage Ⅰ (top) and Ⅲ (bottom) from CRC TMA, as evaluated by FISH. Scale bar, 200 μm. **E** The overall survival of 180 CRC patients in TMA according to the tumoral circZFR levels, as calculated by Kaplan-Meier analysis. **F** Detection of circZFR in serum samples from 83 CRC patients and 83 healthy controls by qRT-PCR. **G** Evaluation of the diagnostic value of serum circZFR by ROC curve. **H** Schematic illustration demonstrating the structure of circZFR, the back-splicing junction sequences were confirmed by Sanger sequencing. **I** The presence of circZFR and linZFR in cDNA and gDNA were amplified by divergent and convergent primers, respectively. **J and K** Levels of circZFR and linZFR in CRC cell lines with or without RNase R or actinomycin D treatment, as detected by qRT-PCR. The p values in **K** were determined by two-way ANOVA. **L** The cellular location of circZFR in HCT116 cells was determined by FISH. Scale bar, 50 μm. The data are presented as the mean ± SD, two-tailed Student's t-tests, *$p < 0.05$, **$p < 0.01$ and ***$p < 0.001$.

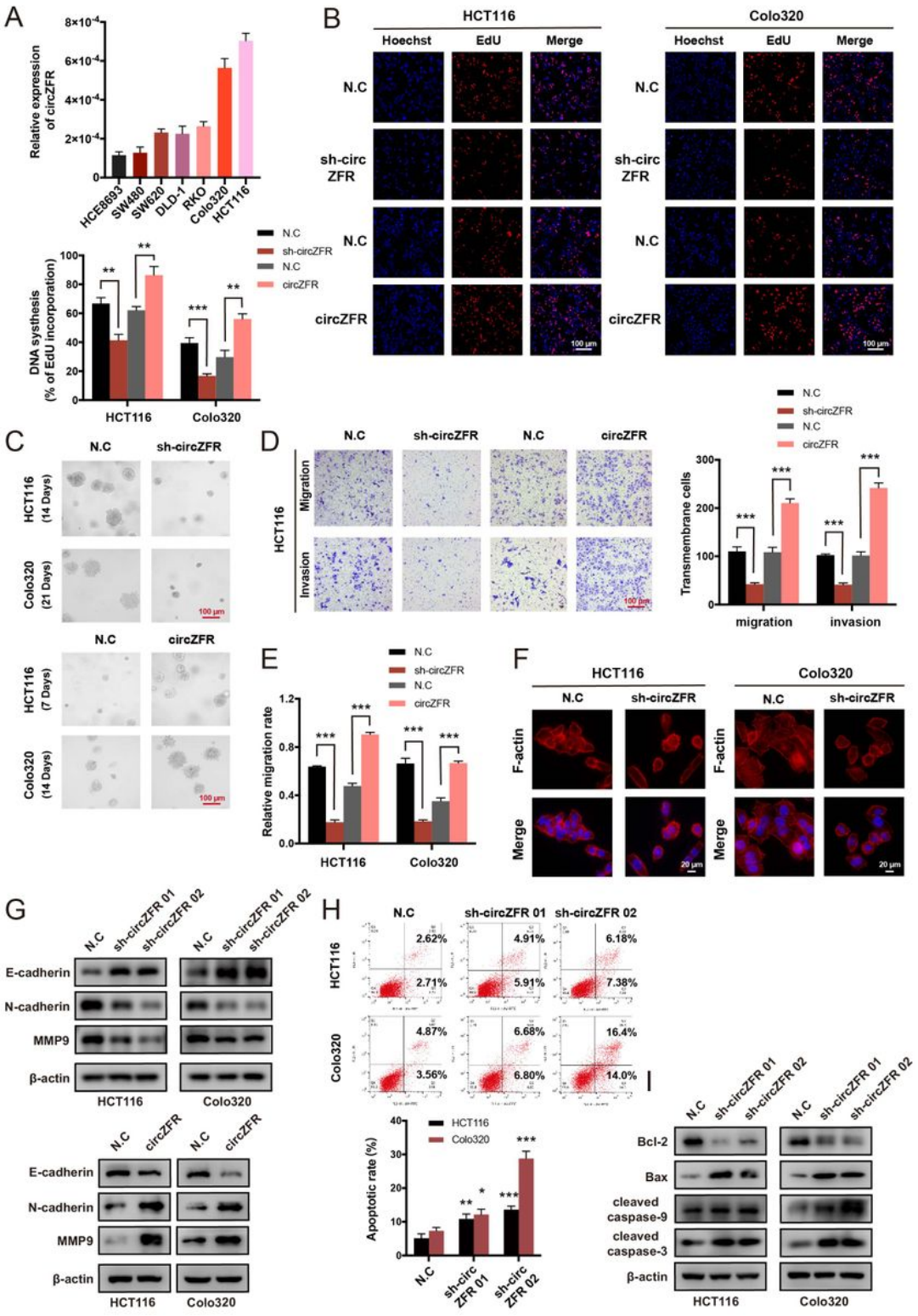

Figure 2

CircZFR promotes proliferation and motility of CRC cells *in vitro*. **A** Levels of circZFR in 7 CRC cell lines, as determined by qRT-PCR. **B and C** The effect of circZFR knockdown and overexpression on CRC cell proliferation, as assessed by EdU and soft agar assays. Scale bar, 100 μm. **D and E** The effect of circZFR knockdown and overexpression on CRC cell migration and invasion, as assessed by Transwell and wound healing assays. Scale bar in Transwell assays, 100 μm. **F** The effect of circZFR knockdown on F-

actin structure of CRC cells, as assessed by cytoskeleton assay. Scale bar, 20 μm. **G** The effect of circZFR knockdown and overexpression on the expression of EMT markers and MMP9, as assessed by Western blotting. **H** The effect of circZFR knockdown on CRC cell apoptosis, as assessed by flow cytometry assay. **I** The effect of circZFR knockdown on the expression of apoptotic markers and caspase proteins, as assessed by Western blotting. The data are presented as the mean ± SD of three independent experiments, two-tailed Student's t-tests, *$p < 0.05$, **$p < 0.01$ and ***$p < 0.001$.

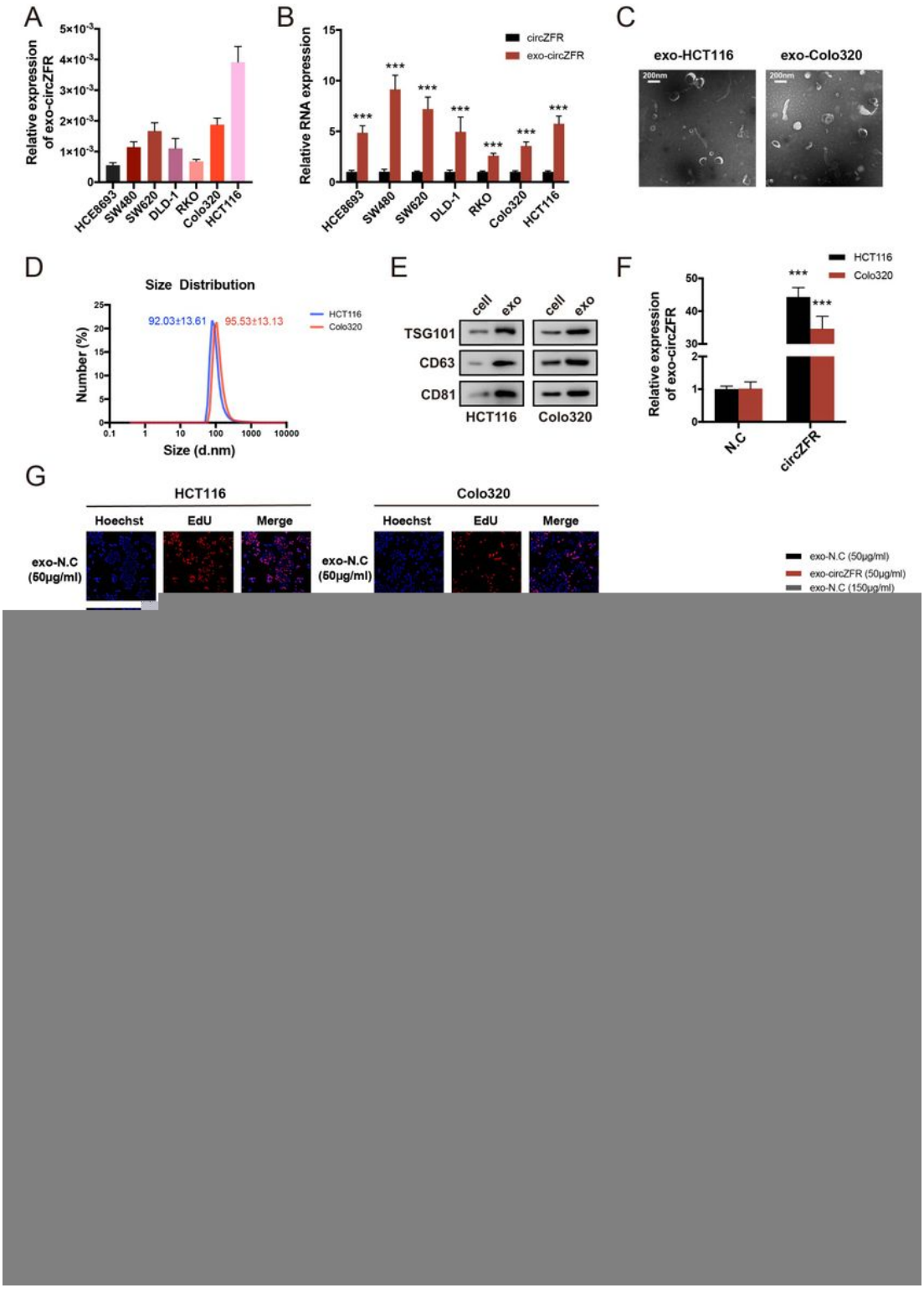

Figure 3

CircZFR can be encapsulated in exosomes to promote CRC cell proliferation and migration. A Levels of circZFR in the medium-derived exosomes of 7 CRC cell lines, as determined by qRT-PCR. **B** Levels of circZFR in 7 CRC cell lines and their medium-derived exosomes, as determined by qRT-PCR. **C, D and E** Identification of medium exosomes from HCT116 and Colo320 cells by TEM, DLS and Western blotting. Scale bar in TEM, 200 nm. **F** Assessment of exo-circZFR levels from CRC cells transfected with N.C or circZFR overexpression plasmid by qRT-PCR. **G** The effect of different concentrations of exo-circZFR from cells transfected with N.C or circZFR overexpression plasmid on CRC cell proliferation, as assessed by EdU assay. Scale bar, 100 μm. **H** The effect of different concentrations of exo-circZFR from cells transfected with N.C or circZFR overexpression plasmid on CRC cell migration, as assessed by Transwell assay. Scale bar, 100 μm. The data are presented as the mean ± SD of three independent experiments, two-tailed Student's t-tests, $*p < 0.05$, $**p < 0.01$ and $***p < 0.001$.

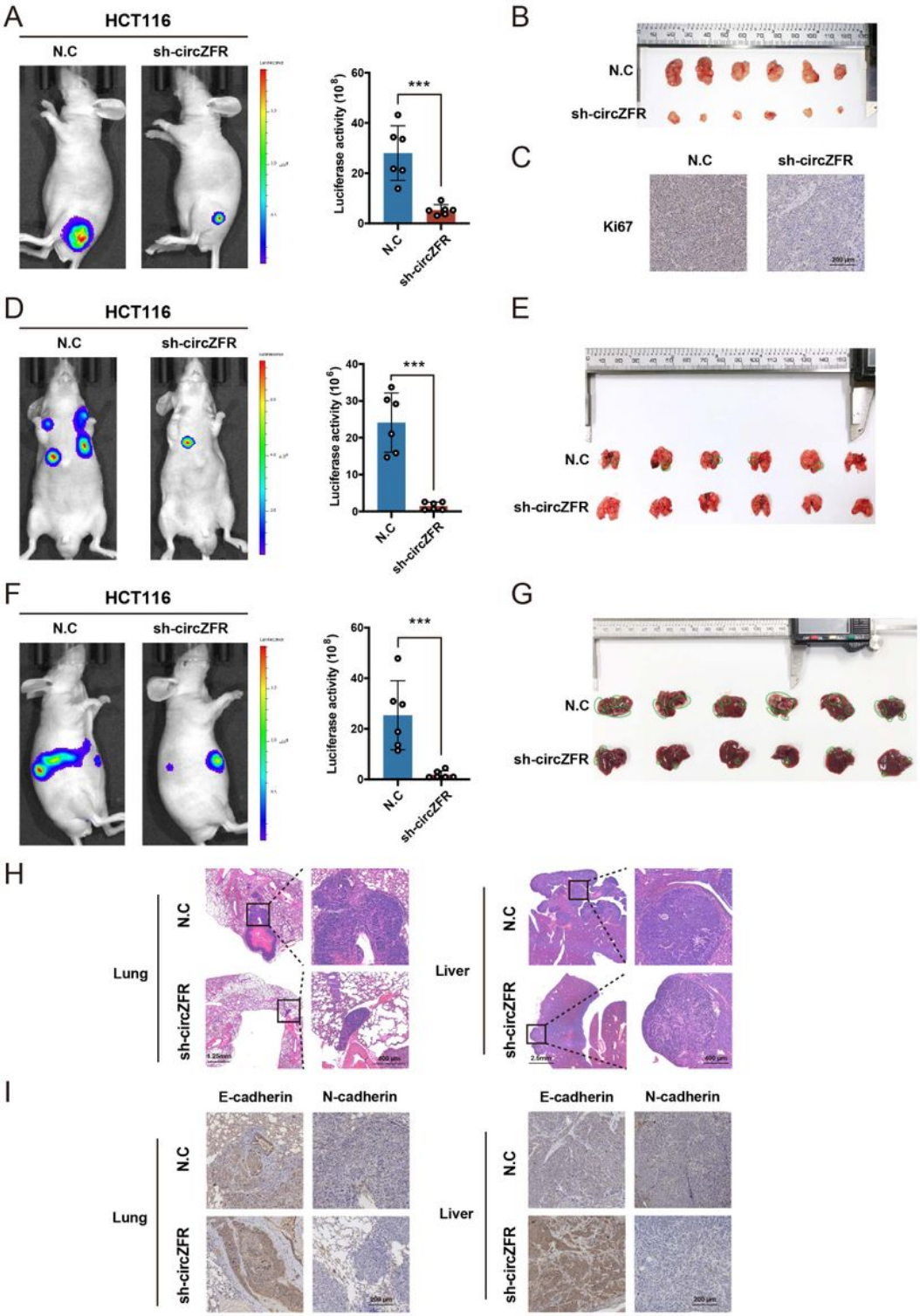

Figure 4

CircZFR promotes CRC growth and metastasis *in vivo*. A and B Representative bioluminescence images and xenograft tumors of mice injected with HCT116 cells transfected with N.C or sh-circZFR plasmid (n = 6) and a histogram showed the luciferase activity. **C** Representative IHC staining images showed the expression of Ki67 in tumors of mice injected with HCT116 cells transfected with N.C or sh-circZFR plasmid. Scale bar, 200 μm. **D and E** Representative bioluminescence images and lung after tail vein

injection of HCT116 cells transfected with N.C or sh-circZFR plasmid (n = 6) and a histogram showed the luciferase activity. The green cycle indicates pulmonary metastases. **F and G** Representative bioluminescence images and liver after spleen injection of HCT116 cells transfected with N.C or sh-circZFR plasmid (n = 6) and a histogram showed the luciferase activity. The green cycle indicates hepatic metastases. **H and I** Representative H&E and IHC staining images showed the mouse metastases and the expression of E-cadherin and N-cadherin in metastases of mice injected with HCT116 cells transfected with N.C or sh-circZFR plasmid. Scale bar, 200 μm. The data are presented as the mean ± SD, two-tailed Student's t-tests, $*p < 0.05$, $**p < 0.01$ and $***p < 0.001$.

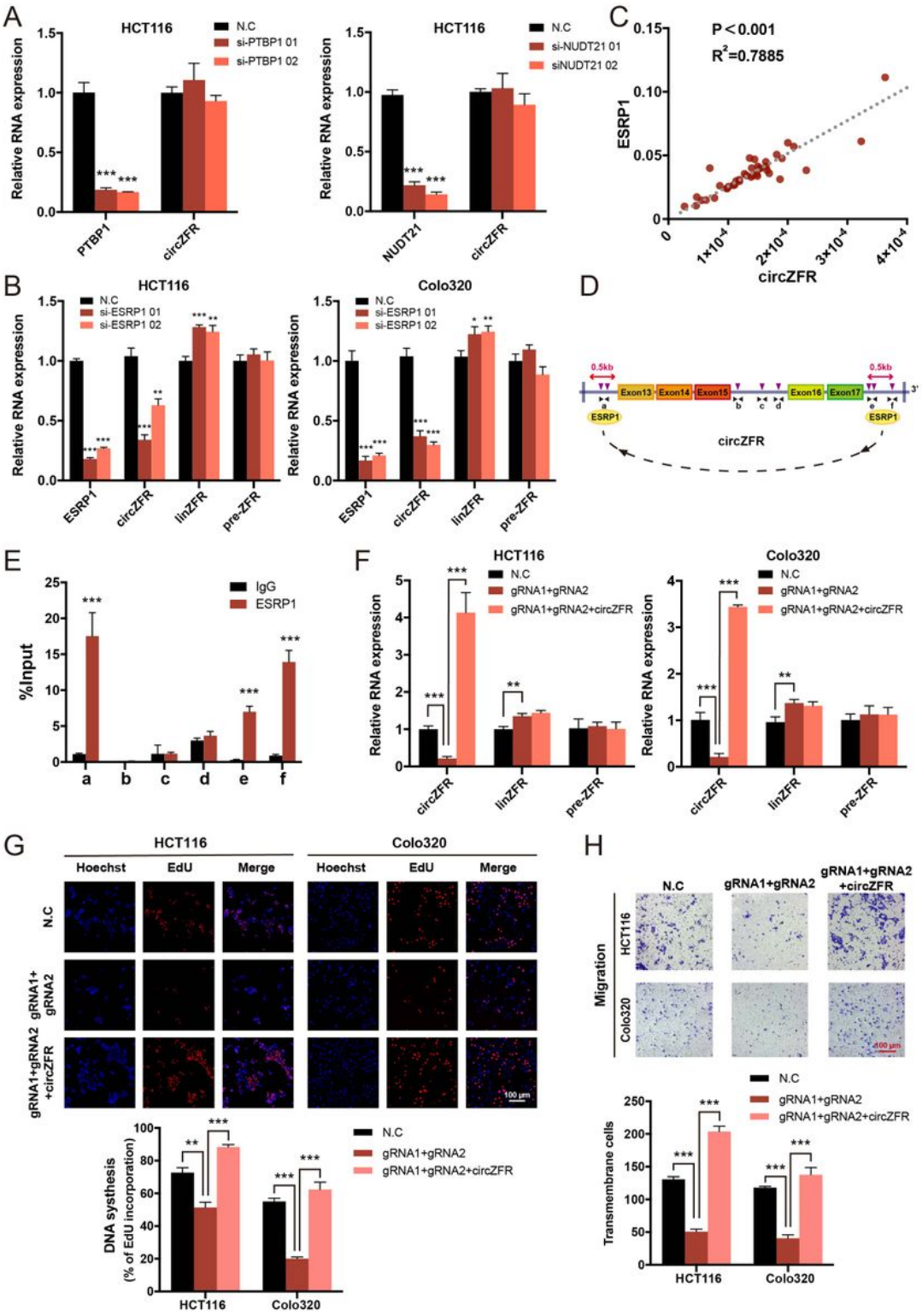

Figure 5

ESRP1 promotes the generation of circZFR in CRC cells. A Levels of PTBP1 or NUDT21 and circZFR in HCT116 transfected with N.C or PTBP1 or NUDT21 siRNAs, as determined by qRT-PCR. **B** Levels of ESRP1, circZFR, linZFR and pre-ZFR in CRC cells transfected with N.C or ESRP1 siRNAs, as determined by qRT-PCR. **C** The correlation between ESRP1 and circZFR expression in 40 CRC tissues, as detected by qRT-PCR. The P values and R^2 values were from Pearson's correlation analysis. **D** Schematic drawing of

specific primers targeting the putative ESRP1-binding sequences on the flanking introns of circZFR. **E** The binding between ESRP1 and the specific sequences on the flanking introns of circZFR, as detected by RIP assay. **F** Levels of circZFR, linZFR and pre-ZFR in CRC cells after CRISPR/Cas9 or co-overexpression of circZFR, as determined by qRT-PCR. **G** Assessment of the proliferation of CRC cells after CRISPR/Cas9 or co-overexpression of circZFR by EdU assay. Scale bar, 100 μm. **H** Assessment of the migration of CRC cells after CRISPR/Cas9 or co-overexpression of circZFR by Transwell assay. Scale bar, 100 μm. The data are presented as the mean ± SD of three independent experiments, two-tailed Student's t-tests, $*p < 0.05$, $**p < 0.01$ and $***p < 0.001$.

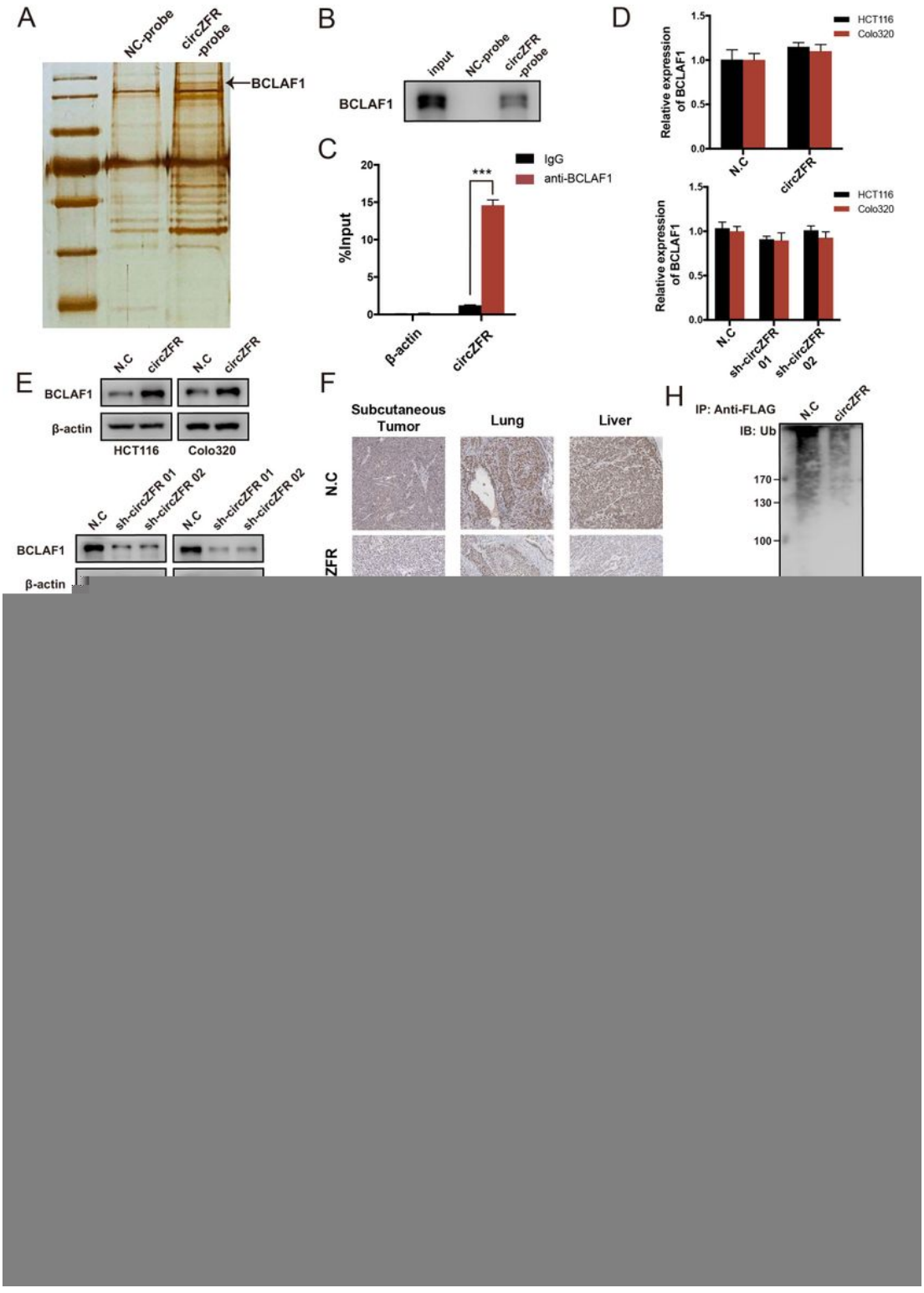

Figure 6

CircZFR binds to BCLAF1 and suppresses its ubiquitinated degradation. A Silver staining of circZFR pulldown. The arrow indicates BCLAF1. **B and C** The combination of circZFR with BCLAF1 in HCT116, as determined by pulldown with Western blotting and RIP assays. **D and E** Levels of BCLAF1 mRNA and protein in CRC cells transfected with N.C, circZFR overexpression or sh-circZFR plasmids, as determined by qRT-PCR and Western blotting. **F** Representative IHC staining images showed the expression of

BCLAF1 in tumors of mice injected with HCT116 cells transfected with N.C or sh-circZFR plasmid. Scale bar, 200 μm. **G** The effect of CHX treatment with or without either MG132 or chloroquine treatment on the expression of BCLAF1 in CRC cells transfected with N.C and circZFR overexpression plasmid, as assessed by Western blotting. **H** The ubiquitination levels of BCLAF1 in N.C and circZFR-overexpressing HCT116 transfected with FLAG-tagged BCLAF1 plasmid after MG132 treatment, as assessed by IP assay. **I** The effect of PR619 treatment on the expression of BCLAF1 in N.C and circZFR-overexpressing CRC cells, as assessed by Western blotting. **J** Assessment of the proliferation of CRC cells after circZFR knockdown or co-overexpression of BCLAF1 by CCK-8 assay. **K** Assessment of the migration of CRC cells after circZFR knockdown or co-overexpression of BCLAF1 by Transwell assay. Scale bar, 100 μm. The data are presented as the mean ± SD of three independent experiments, two-tailed Student's t-tests, $*p < 0.05$, $**p < 0.01$ and $***p < 0.001$.

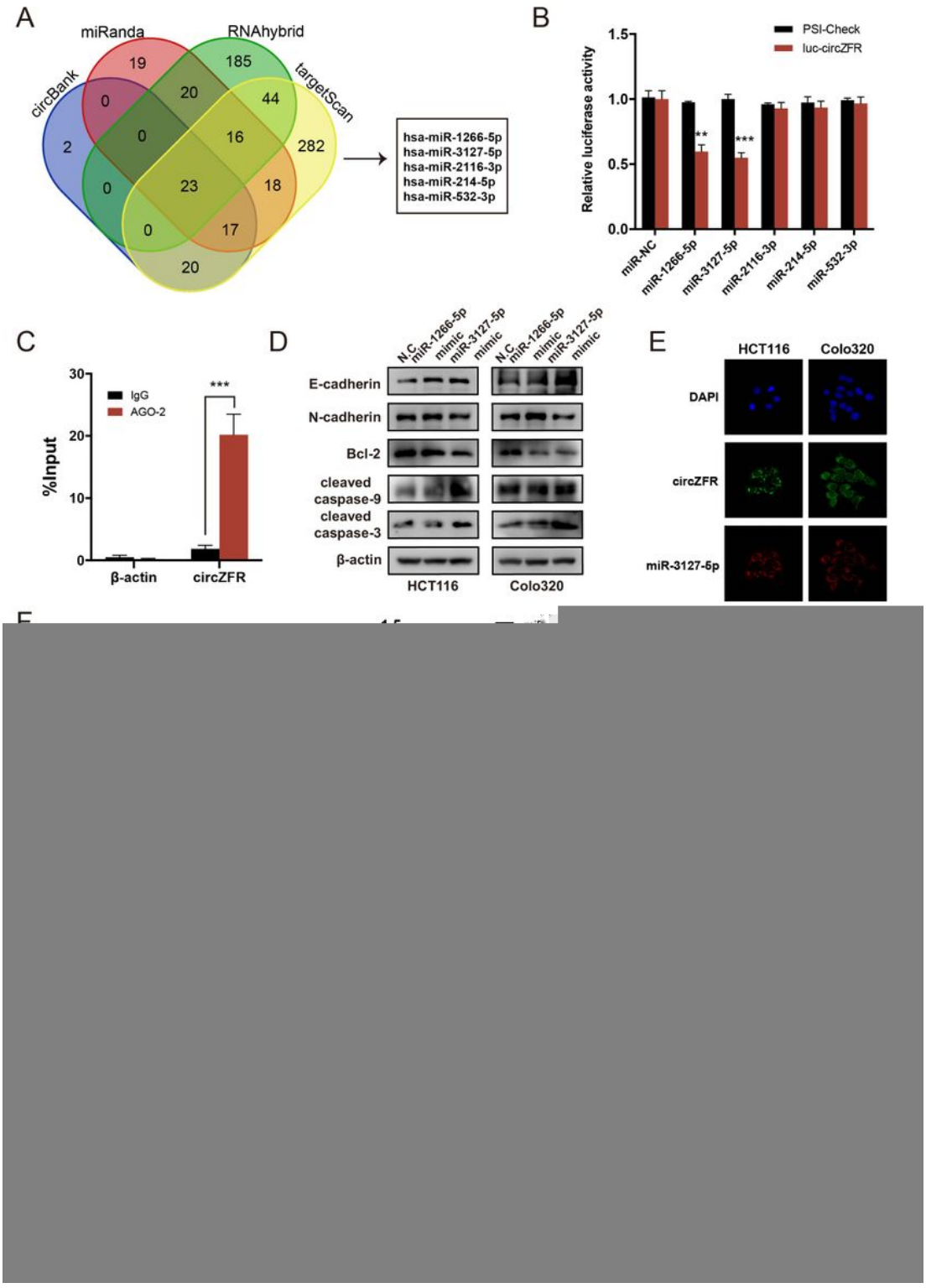

Figure 7

CircZFR serves as a miR sponge for miR-3127-5p. A Venn diagram demonstrating the overlap of the potential target miRs of circZFR predicted by circBank, miRanda, RNAhybrid and targetScan. The arrow indicates five screened candidates according to miR abundance and expression between CRC and normal tissues. **B** Relative luciferase activities in 293T cotransfected with control vector (PSI-Check), circZFR dual-luciferase reporter plasmid and miR mimics, as detected by luciferase reporter assay. **C** The

combination of circZFR with AGO-2 in HCT116, as determined by RIP assay. **D** The effect of miR-1266-5p and miR-3127-5p on the expression of EMT and apoptotic markers and caspase proteins in CRC cells, as assessed by Western blotting. **E** Colocalization of circZFR and miR-3127-5p in CRC cells, as detected by FISH. Scale bar, 20 μm. **F** Schematic graph of potential binding sites of circZFR and miR-3123-5p and relative luciferase activities in CRC cells cotransfected with circZFR-WT or circZFR-MUT and miR-3127-5p mimics or miR-NC, as detected by luciferase reporter assay. **G** Assessment of the proliferation of CRC cells after circZFR or miR-3127-5p individually or simultaneously overexpression by CCK-8 assay. **H** Assessment of the migration and invasion of CRC cells after circZFR or miR-3127-5p individually or simultaneously overexpression by Transwell assay. Scale bar, 100 μm. The data are presented as the mean ± SD of three independent experiments, two-tailed Student's t-tests, $*p < 0.05$, $**p < 0.01$ and $***p < 0.001$.

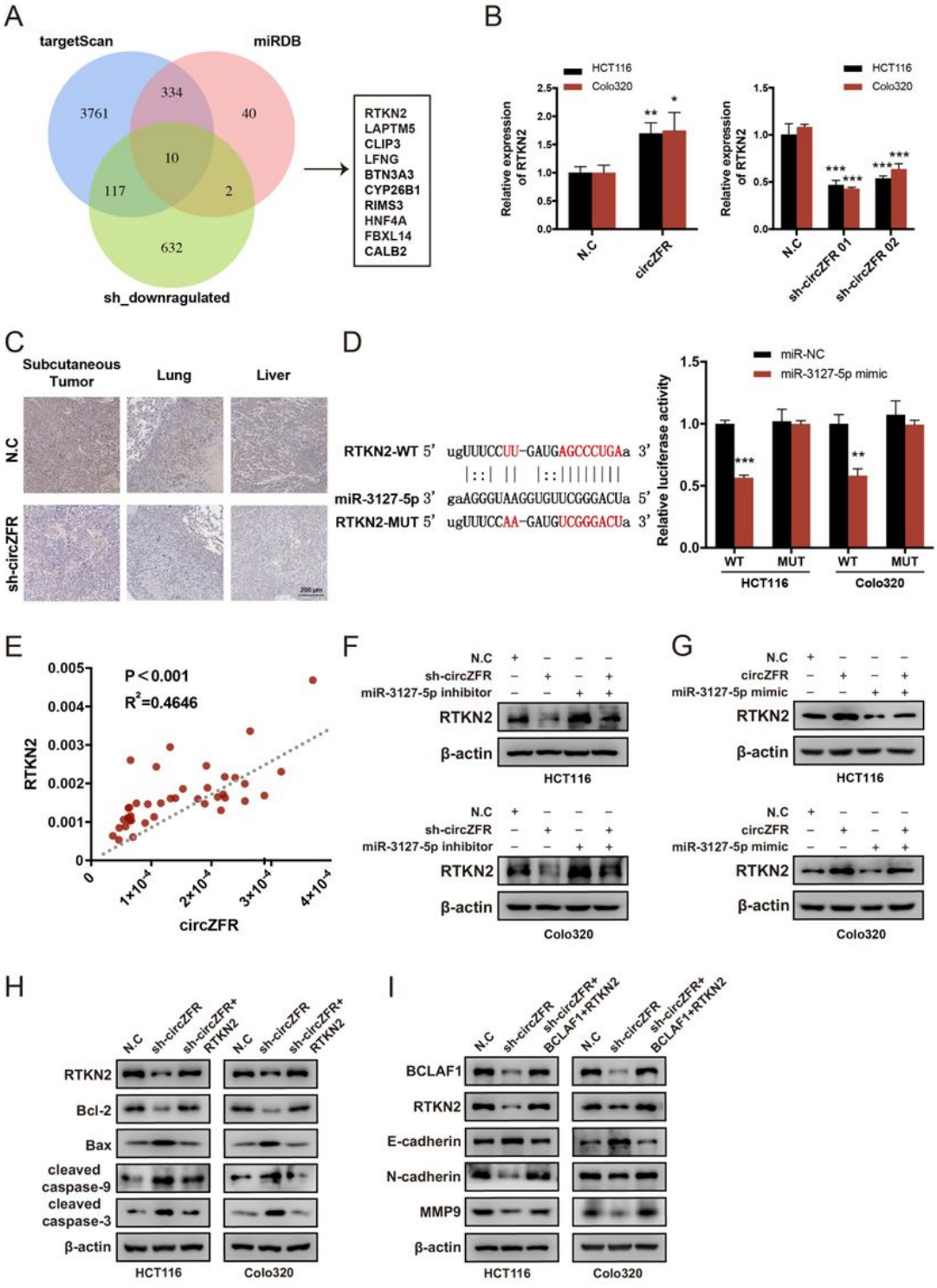

Figure 8

RTKN2 is the direct target of circZFR/miR-3127-5p axis. A Venn diagram exhibiting the overlap between the downregulated mRNAs after circZFR knockdown and the potential targets of miR-3127-5p predicted by targetScan and miRDB. **B** Levels of RTKN2 in CRC cells transfected with N.C, circZFR overexpression or sh-circZFR plasmids, as determined by qRT-PCR. **C** Representative IHC staining images showed the expression of RTKN2 in tumors of mice injected with HCT116 cells transfected with N.C or sh-circZFR

plasmid. Scale bar, 200 μm. **D** Schematic graph of RTKN2 3'UTR-WT and MUT in the miR-3127-5p potential binding sites and relative luciferase activities in CRC cells cotransfected with RTKN2 3'UTR-WT or RTKN2 3'UTR-MUT and miR-3127-5p mimics or miR-NC, as detected by luciferase reporter assay. **E** The correlation between RTKN2 and circZFR expression in 40 CRC tissues, as detected by qRT-PCR. The P values and R^2 values were from Pearson's correlation analysis. **F** Assessment of the RTKN2 levels in CRC cells after circZFR or miR-3127-5p individually or simultaneously knockdown by Western blotting. **G** Assessment of the RTKN2 levels in CRC cells after circZFR or miR-3127-5p individually or simultaneously overexpression by Western blotting. **H** Assessment of the expression of apoptotic markers and caspase proteins in CRC cells after circZFR knockdown or co-overexpression of RTKN2 by Western blotting. **I** Assessment of the expression of EMT markers and MMP9 in CRC cells after circZFR knockdown or co-overexpression of BCLAF1 and RTKN2 by Western blotting. The data are presented as the mean ± SD of three independent experiments, two-tailed Student's t-tests, $*p < 0.05$, $**p < 0.01$ and $***p < 0.001$.

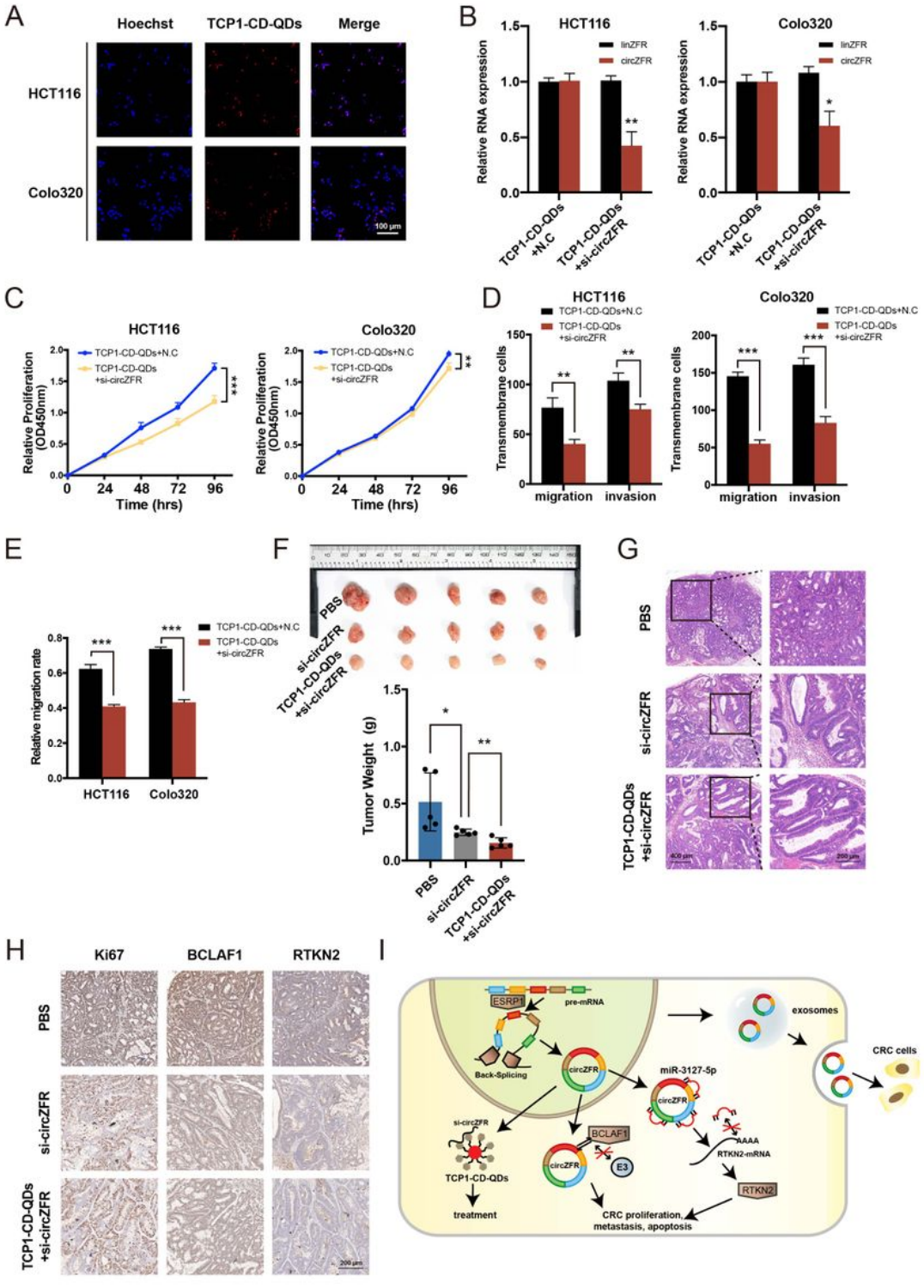

Figure 9

TCP1-CD-QDs loaded with si-circZFR promotes oncogenic phenotypes of CRC cells and PDX tumor growth. A The uptake capacity of CRC cells incubated with TCP1-CD-QDs nanocarriers. Scale bar, 100 μm. **B** Levels of circZFR and linZFR in CRC cells incubated with TCP1-CD-QDs nanocarrier loaded with N.C siRNA or si-circZFR, as determined by qRT-PCR. **C** Assessment of the proliferation of CRC cells incubated with TCP1-CD-QDs nanocarrier loaded with N.C siRNA or si-circZFR by CCK-8 assay. **D and E**

Assessment of the migration and invasion of CRC cells incubated with TCP1-CD-QDs nanocarrier loaded with N.C siRNA or si-circZFR by Transwell and wound healing assays. Scale bar in Transwell assays, 100 μm. **F** PDX tumors of mice after tail vein injection of PBS, si-circZFR or TCP1-CD-QDs nanocarrier loaded with si-circZFR (n = 5) and a histogram showed the tumor weight. **G and H** Representative H&E and IHC staining images showed the PDX tumors and the expression of Ki67, BCLAF1 and RTKN2 in mice after tail vein injection of PBS, si-circZFR or TCP1-CD-QDs loaded with si-circZFR. Scale bar, 200 μm. **I** Schematic diagram illustrating the action of circZFR promoting CRC progression. The data are presented as the mean ± SD of three independent experiments, two-tailed Student's t-tests, *$p < 0.05$, **$p < 0.01$ and ***$p < 0.001$.

Supplementary Files

This is a list of supplementary files associated with this preprint. Click to download.

- Table1.pdf
- FigureS1.jpg
- FigureS2.jpg
- FigureS3.jpg
- FigureS4.jpg
- FigureS5.jpg
- FigureS6.jpg